Effect of metal ions on physical properties of multilayers from hyaluronan and chitosan and adhesion, growth and adipogenic differentiation of multipotent mouse fibroblasts

Husnia Kindi[1], Matthias Menzel[2], Andreas Heilmann[2], Christian E. H. Schmelzer[2], M. Herzberg[3], Bodo Fuhrmann[4, 7], Gloria Gallego-Ferrer[5, 6], Thomas Groth[1, 7, 8]

[1]Department Biomedical Materials, Institute of Pharmacy, Martin Luther University Halle-Wittenberg, 06120 Halle (Saale), Germany.

[2]Department of Biological and Macromolecular Materials, Fraunhofer Institute for Microstructure of Materials and Systems IMWS, 06120 Halle (Saale), Germany.

[3]Molecular Microbiology, Institute for Biology/Microbiology, Martin-Luther-University, Halle-Wittenberg, Germany.

[4]Institute of Physics, Martin Luther University Halle–Wittenberg, 06099 Halle (Saale), Germany.

[5]Centre for Biomaterials and Tissue Engineering, Universitat Politècnica de València, Caminode Veras/n, 46022 Valencia, Spain.

[6]Biomedical Research Networking Centre in Bioengineering, Biomaterials and Nanomedicine (CIBER-BBN), 46022 Valencia, Spain.

[7]Interdisciplinary Center of Materials Science, Martin Luther University Halle-Wittenberg, 06120 Halle (Saale), Germany.

[8]Laboratory of Biomedical Nanotechnologies, Institute of Bionic Technologies and Engineering, I.M. Sechenov First Moscow State University, 119991, Trubetskaya street 8, Moscow, Russian Federation

Abstract

Polyelectrolyte multilayers (PEM) consisting of the polysaccharides hyaluronic acid (HA) as polyanion and chitosan (Chi) as polycation were prepared by the layer-by-layer technique (LbL). The $[Chi/HA]_5$ multilayers were cross-linked by metal ions (Ca^{2+}, Co^{2+}, Cu^{2+} and Fe^{3+}). Binding of metal ions to $[Chi/HA]_5$ multilayers can cause coordination-based intrinsic cross-linking of functional groups of polysaccharides, which modulated physical properties and bioactivity of PEM with regard to the adhesion and function of multipotent murine C3H10T1/2 embryonic fibroblasts. Characterization of multilayer formation and surface properties using different analytical methods demonstrated changes in wetting, thickness and mechanical properties of multilayers depending on the concentration and type of metal ion. Most interestingly, we found that Fe^{3+} metal ions promoted adhesion and spreading of C3H10T1/2 cells greatly on the low adhesive $[Chi/HA]_5$ PEM system. The intrinsic cross-linking by intermediate concentrations of Cu^{2+}, Ca^{2+} and Co^{2+} as well as low concentrations of Fe^{3+} also resulted in increased cell spreading. Moreover, it was shown that cross-linking of multilayers with Cu^{2+} and Fe^{3+} ions led to increased metabolic activity in cells after 24 h and induced cell differentiation towards adipocytes in the absence of any additional adipogenic media supplements. Overall, cross-linking of $[Chi/HA]_5$ PEM with metal ions represents an interesting and cheap alternative to the use of growth factors for making cell-adhesive coatings and guide stem cell differentiation on implants and scaffolds to regenerate connective type of tissue.

Keywords:

Chitosan, hyaluronic acid, intrinsic cross-linking, metal ions, mesenchymal stem cells, cell adhesion, CD44, adipogenic differentiation.

1. Introduction

Chemical and physical surface modifications are frequently utilized to adapt biomaterials to specific medical applications such as blood or tissue contact to achieve the required biocompatibility and performance of a biomedical device [1]. The precise control of bulk and surface properties of biomaterials at micro- or nanometer scale to direct cell fate is still a great challenge. Properties like wettability, surface charge and topography influence the adsorption of proteins (e.g. from blood or tissue fluid) with potential effects on their bioactivity [1] and subsequent adhesion, growth and differentiation of cells [2]. Moreover, the release of bioactive molecules from scaffolds and implants [3] or surface coatings of medical devices [4] is proposed as a tool to control cell differentiation in the desired direction.

A physical surface modification widely done is the layer-by-layer (LbL) method, which is based on the alternating deposition of macromolecules of opposite net charge by electrostatic attraction and ion-pairing on a charged substrate [5]. The generation of polyelectrolyte multilayers (PEMs) by other interactions such as van-der-Waals forces, hydrogen bonding and hydrophobic interactions are also exploited in LbL assembly [6-7]. Multilayer properties like thickness, wettability, surface charge, topography and viscoelastic properties can be controlled by choice of macromolecular entities and complexation conditions [8]. Recently, intrinsic cross-linking of multilayers by chemical means or coordination-based chemistry has been suggested as well with effects on stability and mechanical properties of multilayers [8-9]. An interesting aspect of LbL technique is that many biomolecules such as proteins and glycosaminoglycans (GAGs) represent polyelectrolytes and can therefore be used for multilayer formation that may lead to surface coatings mimicking the microenvironment of cells [10].

Cells in tissues are connected to and interact with the extracellular matrix (ECM), a well-organized system made of proteins and polysaccharides (e.g. collagens and proteoglycans with GAGs) that provide mechanical and chemical cues to cells [11]. The interaction between cells and ECM proteins is driven mainly by integrins as cellular adhesion receptors for proteins like collagen, elastin, fibronectin and others [12], but also by cell hyaladherin receptors like CD44 for

the GAG hyaluronan[13]. By contrast, other GAGs such as heparan sulfate or chondroitin sulfate form bridges between matrix proteins and cell receptors as part of matrix- or cell surface-proteoglycans, but are also involved in storage and presentation of growth factors and other cytokines [14]. Overall, the binding of these ligands to cell receptors transmits both chemical and mechanical signals that regulate adhesion, migration, growth, and differentiation of cells.

Mesenchymal stem cells (MSCs) are promising candidates for tissue engineering and regenerative medicine due to their capability to differentiate into multiple cell types, such as adipocytes, chondrocytes, osteocytes and others [15-16]. It was observed that the composition of substrata, degree of cell spreading and presence of ECM proteins and cytokines can control the development of these cells in specific lineages like adipocytes, osteoblasts or chondrocytes [17]. Besides, these chemical cues, viscoelastic properties of substrata have been found to control their differentiation[18]. One obstacle for clinical application and fundamental studies of MSC is their limited proliferation capacity to only a few *in vitro* passages of explanted cells. Hence, multipotent cell lines like C3H10T1/2 mouse fibroblasts have attracted attention for fundamental studies, since they possess the potential to differentiate into several cell lineages in response to stimuli like growth factors, having at the same time a high proliferative capacity [19].

Although multitudes of studies were done on the effect of growth factors, the effect of metal ions on growth and differentiation of MSC represents another opportunity to control their fate. Metal ions represent not only basic components of tissues like calcium in bone but play also numerous roles for the function of proteins, cells and organs that have been reviewed here [20] [21]. Metal ions found to be an important role during different steps of bone regeneration as highlighted by Glenske et al. [22]. For example, calcium ions enhance proliferation and differentiation of MSC by activation of calcium receptors [23]. Cobalt ions are known to have the capacity to promote angiogenesis by activating hypoxia-inducible transcription factors (HIF-1α) and subsequently the production of vascular endothelial growth factor (VEGF), which enhances the osteogenic differentiation of cells [24]. Copper ions can not only inhibit the growth

of bacteria and stimulate biological responses in mesenchymal stem cells (MSC) by increasing the expression of VEGF and HIF-1α [25], they are also involved in the regulation of bone metabolism [22] and are essential to stimulate collagen fiber deposition and blood vessel formation [26]. Iron plays important roles in a variety of cellular processes such as the synthesis of DNA, RNA, protein functions like hemoproteins, electron transfer processes in mitochondria, cellular proliferation and osteogenic differentiation [27 28].

Metal ions like calcium, copper, cobalt, iron and others can bind to proteins, polysaccharides and other organic molecules both through ionic interaction to charged groups like carboxylic functions, in addition but also coordinative bonds to nitrogen in amino, and oxygen in hydroxyl and carbonyl groups [29]. Hence, metal ions may also be used for cross-linking polyelectrolytes by these type of bonds, which may affect the physical properties of multilayers, but potentially also the biological response and differentiation of cells. Hence, we studied here the effect of exposition of PEM made of hyaluronan as polyanion and chitosan as polycation to calcium, cobalt, copper and iron ions on the physical properties of multilayers and the biological response of multipotent embryonic mouse fibroblasts (C3H10T1/2) in terms of cell adhesion, growth and adipogenic differentiation.

2. Materials and methods

2.1 Materials

Circular glass cover slides (Menzel, Bielefeld, Germany) of 12 mm in diameter and silicon wafers (Silicon materials, Kaufering, Germany) of (10x10) mm² and (37×17) mm² were used as substrata for deposition of multilayers. They were treated according to RCA clean I cleaning protocol [30], using a solution of ammonia 25% and hydrogen peroxide 35% (Roth, Karlsruhe, Germany) and water (1:1:5, v/v/v) heated to 75 °C. All samples were immersed for 15 min in this solution, subsequently washed with ultrapure water, and dried with a stream of nitrogen. New gold-coated sensors for surface plasmon resonance studies (SPR, IBIS Technologies B.V, Enschede, Netherlands) were rinsed with ethanol (p.a., Roth) and distilled water. After drying with nitrogen, the cleaned gold sensors were incubated in 2 mM mercaptoundecanoic

acid (MUDA, 95%, Sigma, Germany) in ethanol (p.a.) overnight to obtain a negatively charged surface due to presence of terminal carboxyl groups [31].

A solution of chitosan (Chi, Mw = 5500 kDa, 85/500/A1, Heppe Medical Chitosan, Halle, Germany) with a deacetylation degree of 85% was prepared by dissolution in 0.15 M NaCl at a concentration of 1 mg/mL under stirring. Acetic acid (0.05 M) was added to the Chi solution, which was heated to 50 °C for 2 h, followed by adjustment of pH to 4.0 by dropwise addition of 0.1 M sodium hydroxide. Hyaluronic acid sodium salt from Streptococcus equi (HA, Mw ~1.5-1.8 MDa, Sigma, Germany), was dissolved in 0.15 M NaCl pH 4.0 at a concentration of 1 mg/mL. The metal salts calcium chloride dihydrate ($CaCl_2$, Mw = 147.03 g/mol), cobalt chloride hexahydrate 99%, p.a. ($CoCl_2$, Mw = 237.93 g/mol) (Roth, Karlsruhe, Germany), copper (II) chloride dihydrate 99%, p.a. ($CoCl_2$, Mw = 170.48 g/mol), and iron (III) chloride hexahydrate 99%, p.a. ($FeCl_3$, Mw = 270.33 g/mol) were dissolved in ultrapure water at concentrations of 5, 10 and 50 mM, while the pH was adjusted to 4.0 by dropwise addition of 0.1 M hydrochloric acid. Iron (III) chloride could not be used at 50 mM because of precipitation of the salt at this high concentration, when the solution pH was adjusted to pH 4.0.

2.2 Polyelectrolyte multilayer (PEM) formation.

Multilayer films were fabricated on cleaned substrates (glass or silicone) by alternating adsorption of Chi and HA (concentration 1 mg/mL in 150 mM NaCl, pH 4.0) up to 5 bilayers were obtained. The multilayer system was denominated as $[Chi/HA]_5$. Each layer was formed by immersing the substrates in 1 mL of polyelectrolyte solutions for 15 min, followed by rinsing with 1 mL 0.15 M sodium chloride solution (pH 4.0) for three times 5 min. Afterwards, the multilayers were placed in 1 mL metal ion solutions (Ca^{2+}, Co^{2+}, Cu^{2+}, and Fe^{3+}) of different concentration (5, 10, and 50 mM) for 15 min followed by three times rinsing with 0.15 M NaCl for 5 min each. The resulting multilayers are then denominated as $[Chi/HA]_5$ -Me_c, where Me stands for the type of metal ion and subscript C for its concentration.

2.3 Characterization of multilayer formation, uptake of metal ions and surface properties

2.3.1 Surface Plasmon Resonance (SPR)

SPR was applied to study the growth behaviour of multilayer films on gold-coated glass sensors using the IBIS-iSPR equipment (IBIS Technologies B.V, Enschede, Netherlands). A change in the angle shift of the incident light (m°) of SPR is proportional to the mass (Γ_{SPR}) of adsorbed molecules on the surface [32]. A new, MUDA-modified gold sensor was placed into the iSPR the flow cell, which was equilibrated with degassed 0.15M NaCl pH 4.0 to obtain a stable baseline. Subsequently, multilayers were assembled as described above using a flow rate of 3 mL/min at 25 °C.

2.3.2 Ellipsometry

The thickness of PEM was determined by multispectral ellipsometry (M-2000V, J.A. Woollam Company, Lincoln, NE; USA) under dry and wet conditions. At dry conditions, PEMs were assembled separately on silicon wafers in vitro and allowed to dry in a desiccator at least overnight. Afterwards, the samples were placed in the ellipsometry and scanned with an angle range of 65° to 85°. At least three samples were studied by measuring five spots on each sample. For wet conditions, ellipsometry was equipped with a liquid cell and PEM formation was studied in situ. Therefore, the silicon slides were mounted inside the 500 µL liquid cell and polyelectrolytes Chi and HA and washing solutions were pumped subsequently through the cell. The surface was scanned at a static angle of 70°. The in situ experiments were run in triplicate. The thickness of PEM was obtained by fitting the experimental data to an additional Cauchy layer, while a refractive index of 1.4 was used for PEM thickness calculation, which is recommended for native polysaccharides [33]. The experimental data were analysed by using the onboard software Wvase32.

2.3.3 Inductively-coupled plasma mass spectrometry (ICP-MS) analysis

To determine the metal content via ICP-MS analysis, the multilayer-coated wafers/glasses were immersed in concentrated 67% (w/v) HNO_3 (trace metal grade; Normatom / ProLabo) at

70 °C for 2 h. Samples were diluted to a final concentration of 5-6% (w/v) in nitric acid. Indium and germanium (VWR Merck / VWR chemicals) were added as internal standards at a final concentration of 2 / 20 ppb and 5% isopropanol (Sigma). Elemental analysis was performed via inductively-coupled plasma mass spectrometry (ICP-MS) using a Cetac ASX-560 (Teledyne, Cetac Technologies, Omaha USA), a MicroFlow PFA-200 nebulizer and an iCAP-RQ ICP-MS instrument (Thermo Fisher Scientific, Bremen) operating with a collision/reaction cell and flow rates of 5 mL/min of He/H_2 (93% / 7% [13,3:1]), with an Ar (4.8) carrier flow rate of 0.72 L/min and an Ar (4.8)-plasma makeup flow rate of 15 L/min. Data acquisition for each sample was done in triplicate using Qtegra Version 2.10.3324.83 software (Thermo Fisher Scientific). An external calibration curve was recorded with ICP-multi-element standard solution XVI (Merck) or ICP-single-element standards (Merck / Perkin Elmer) in 5% nitric acid. The sample was introduced via a peristaltic pump and analysed for calcium (Ca43), iron (Fe56) cobalt (Co59), copper (Cu63) and other element contaminations in triplicates. For blank measurement and quality/quantity threshold calculation based on clean substances (glass) and original multilayers were used. The results were transformed from ppb sample volume-dependent into ng metal per area (cm^2). By means of the molecular mass of the measured elements a conversion to molar quantities (µmol) was done as well.

2.3.4 FTIR Spectroscopy

The chemical composition of polysaccharides contained in a 100 bilayers of Chi and HA multilayer with metal ions (at highest concentrations used here) were analysed by Fourier transform infrared (FTIR) spectroscopy (IFS 28, Bruker, Germany) after freeze-drying of PEMs. Data from 24 scans with resolution of 4 cm^{-1} were collected in the mid-IR region (4000–400 cm^{-1}). Details of the preparation of freestanding films that were prepared by detachment of PEM from glass substrata can be found in the **Supporting Information**.

2.3.5 Water contact angle studies

Static contact angle (CA) measurements were used to determine the wettability of multilayer surfaces using an OCA15+ device (Dataphysics, Filderstadt, Germany). Here, the captive

bubble technique was used to determine the contact angle of an air bubble on the PEM surfaces. The samples were immersed in a deionised water filled glass chamber and an air volume of 3 µL was dispensed with a flow rate of 1 µL/ s, while the ellipse-fitting method was used to fitting approximation. The experiments were run in triplicate and five bubbles per sample were measured.

2.3.6 Streaming potential measurements

The zeta (ζ) potential of multilayer surfaces was measured with a SurPASS device (Anton Paar, Graz, Austria). Glass coverslips with specific dimensions were used as substrata for multilayer formation that was done by dip-coating before the zeta potential studies as described in section 2.2. Two identical PEM-modified glass coverslips were fixed on stamps and placed oppositely into the adjustable flow cell. The gap was adjusted to a distance where a flow rate of 100-150 mL/min was achieved at a maximum pressure of 300 mbar. Potassium chloride (1 mM) was used as an electrolyte and 1 M sodium hydroxide was used for pH titration. The measurements were performed by an automated titration program from pH 2.5 to 10.0 using volume increments of 20 µL for adjustment of pH values in 0.25 pH steps. Nitrogen was used to purge the buffer solution during measurement. All experiments were run in duplicate.

2.3.7 Atomic force microscopy and nanoindentation

The surface morphology of PEM prepared on cleaned silicon wafers was investigated by atomic force microscopy (AFM). A Nanowizard® IV (JPK/Bruker, Berlin, Germany) was used to determine topography in ambient air using fast nanoindentation (Quantitative Imaging™-Mode), and mechanical properties in intermittent contact mode in a standard liquid cell (JPK/Bruker) with 150 mmol L^{-1} NaCl (pH 4). Here the AFM investigations were carried out to measure a section of 2.5 x 2.5 μm^2 with a resolution of 512 x 512 $pixel^2$ to represent morphological nature of the layers as well as the elastic modulus. The force constant calibration of used standard silicon cantilevers was performed by using the thermal noise method [34]. The AFM probe tip was verified twice-using scanning electron microscopy. First to

measure the radius of the indenter and second to prove tip geometry consistency after completing all measurements. In the post-processing procedure Young´s moduli were calculated from the indentation curves using the advanced Hertzian model [35].

2.4 Biological investigations

2.4.1 Measurement of serum protein adsorption

The capability of PEM to bind serum proteins was quantified by a bicinchoninic acid assay (BCA) (Pierce, ThermoFisher Scientific, Germany). Briefly, PEMs were fabricated in 96 well plates (Greiner Bio-One) according to the protocol described in section 2.2. Then, 250 µL of Eagle's Basal Medium (EBM) supplemented with 10% fetal bovine serum (FBS, Biochrom, Berlin, Germany) were added to the PEM, which were then incubated at 37 °C for 4h. After incubation, the medium was aspirated, and the wells were washed twice with phosphate buffered saline (PBS) pH 7.4. Thereafter, 250 µL of BCA working reagent was added to each well and allowed to react at 37 °C for 30 min. Afterwards, 225 µL of supernatant were transferred from each well into a new 96-well plate, followed by measuring the absorbance at 562 nm with a plate reader (FLUOstar, BMG LabTech, Ortenberg, Germany). The amount of adsorbed protein was calculated from a calibration curve obtained with bovine serum albumin (BSA, Roth).

2.4.2 Cell Culture

Cryopreserved embryonic mouse mesenchymal stem cells (C3H10T1/2, clone 8, ATCC, USA) were thawed and grown in Eagle's Basal medium (EBM) supplemented with 2 mM L-glutamine, 1.5 g/L sodium bicarbonate, Earle's salts, 10% FBS and 1% penicillin/streptomycin (pen/strep, Promocell, Germany) at 37 °C in a humidified 5% CO_2/ 95% air atmosphere. Cells of almost confluent cultures were washed once with sterile PBS pH 7.4 followed by treatment with 0.25% trypsin/0.02% EDTA (Biochrom, Berlin, Germany) at 37 °C for a maximum of 5 min to detach the cells. Trypsin was neutralized with EBM containing 10% FBS, and the cells were resuspended in EBM after centrifugation at 250 *g* for 5 min. Afterward, the cells were seeded on plain and PEM-modified round glass coverslips at a density of 5×10^4 cells/mL.

2.4.3 Immunostaining of cells

C3H10T1/2 cells cultured in the presence of 10% FBS in EBM were cultured on sterilized PEM at 37 °C in a humidified 5% CO_2/ 95% air atmosphere for 4 and 24 h. Adherent cells were fixed with 4% paraformaldehyde solution (Roti® Histofix, Roth) at room temperature for 15 min and washed briefly with PBS, pH 7.4. Then, cells were permeabilized with 0.1% (v/v) Triton X-100 (Sigma) for 10 min. After rinsing twice with PBS, nonspecific binding sites were blocked with 1% BSA in PBS. Focal adhesions were visualized by incubation with a mouse monoclonal antibody raised against vinculin (7F9) (1:50, Santacruz Biotechnology). CD44; the cell-surface receptor of HA, was stained by incubation with a mouse monoclonal antibody raised against CD44 (Dianova, Hamburg, Germany). Specific monoclonal antibody binding was detected by incubation with a goat Cy2-conjugated anti-mouse secondary antibody (1:100, Dianova, Hamburg, Germany). The actin cytoskeleton was visualized by incubating with BODIPY® -phalloidin (1:1000, Invitrogen, Germany) while the nucleus was visualized with TO-PRO 3 (1: 500 Invitrogen). All incubations were performed at room temperature for 30 min followed by extensive washing with PBS three times. The samples were finally mounted to object holders using Mowiol (Calbiochem, Germany) and examined by confocal laser scanning microscopy (CLSM 710, Carl Zeiss Micro-Imaging GmbH, Jena, Germany) using a 10X, 20X, 40X and a 63X oil immersion objective. CLSM images 710 (Carl Zeiss) were used to determine the cell count and cell morphology in terms of cell area and aspect ratio of cells stretching. All data were calculated by Fiji ImageJ.

2.4.4 Cell Growth

For cell growth studies, PEMs were also assembled in 96-well tissue culture plates. Before cell culture, the PEM were sterilized in a UV chamber (Bio-Link BLX, LTF Labortechnik, Germany) at 254 nm (50 J/cm) for 30 min. C3H10T1/2 cells were seeded on PEM at a density of 5×10^4 cells/mL in EBM supplemented with 10% FBS and 1% pen/strep and incubated at 37 °C in a humidified 5% CO_2/95% air atmosphere for 24 and 72 h. The cell morphology and growth was visualized by phase contrast microscopy with an Axiovert 100 (Zeiss) equipped

with a CCD camera (AVT HORN). The quantity of viable cells was measured using the non-toxic QBlue® assay (BioChain, Newark, CA, USA), which is related to the metabolic activity of living cells. The old medium was carefully aspirated and 200 µL of pre-warmed EBM containing the QBlue reagent (ratio 1:10) was added. After additional incubation at 37 °C for 3 h, 100 µL supernatant from each well were transferred to a black 96-well plate (Greiner bio-one, Germany). The fluorescence intensity was measured at an excitation wavelength of 544 nm, while an emission wavelength of 590 nm was used in a plate reader (FLUOstar, BMG LabTech, Germany). The EBM/QBlue solution without cell contact was used as a blank.

2.4.5 Cell differentiation

C3H10T1/2 cells were seeded on original $[Chi/HA]_5$ multilayers and cross-linked metal ions high concentration and cultured with and Dulbecco's Modified Eagle's Medium (DMEM; low-glucose concentration) (Sigma-Aldrich, Germany) supplemented with 10% FBS and 1 % pen/strep at a density of 50 000 cell mL^{-1} for 48 h to obtain a certain degree of confluency. Cells were then incubated for 21 days, while the media were changed twice per week. Adipogenic differentiation efficacy was determined by staining the cells with oil red to estimate the formation of neutral fats in the cytoplasm. Oil red stock solution was prepared by dissolving oil red powder (Sigma-Aldrich, Germany) in isopropanol (Roth, Germany) to achieve a concentration of 0.5% (w/v) during gentle heating. Oil red working solution was prepared by diluting the stock solution with PBS pH 7.4 at a ratio of 3:2. Fixed cells were incubated with filtered oil red working solution in the dark for 30 min. Thereafter, cells were rinsed three times with distilled water and dried in air. All cells were imaged using bright-field microscopy (Leica, Germany). Finally, the cells were stained for specific markers for of adipogenic (perilipin and GLUT4). Later, the cells were rinsed with PBS and fixed with 4% paraformaldehyde (Roti® Histofix, Roth) solution at room temperature for 15 min and washed with PBS. After permeabilization using 0.1% (v/v) Triton X-100 (Sigma- Aldrich) for 10 min, the non-specific binding sites were blocked with a 1% bovine serum albumin solution (BSA; Roth, Germany) in PBS at room temperature for 1 h. For visualization of adipogenic markers, the cells were incubated

with primary monoclonal antibodies raised against perilipin (rabbit) and glucose transporter 4 (GLUT4, mouse) (1:100, sc-biotechnology, Germany) and conjugated secondary anti-mouse (CY2) and anti-rabbit (CY3) antibodies respectively. The actin cytoskeleton was visualized by incubating with BODIPY®-phalloidin (1:1000, Invitrogen, Germany). The samples were examined with confocal laser scanning microscopy (CLSM 710, Carl Zeiss Micro-Imaging GmbH, Jena, Germany) using 40x oil immersion objective. CLSM images 710 (Carl Zeiss).

2.5 Statistics

All data were expressed as mean values ± standard deviations (SD). Statistical analysis was carried out using Origin 8 software. A one-way ANOVA followed by posthoc Tukey's test was performed to estimate the statistical significance of results for $p \leq 0.05$, which is indicated with an asterisk in the respective figures where applicable. Further, the box-whisker plots in panels (b) and (c) indicate the 25^{th} and 75^{th} percentile, the median (dash) and mean values (black square), respectively, whereas the 95%-1% confidence interval is represented by the whiskers.

3. Results and Discussion

3.1. Characterization of multilayer formation and uptake of metal ions

Characterization of multilayer formation and surface properties were performed to study the effects of exposure of $[Chi/HA]_5$ multilayers to metal ions on physical properties of multilayers and to understand whether such changes can explain differences in behavior of cells. The surface sensitive analytical techniques SPR and ellipsometry were used here to monitor the multilayer growth and thickness of $[Chi/HA]_5$ as shown in **Figure 1**. There was a nearly linear increase in SPR angle shift (m°) with the addition of each layer of polyelectrolytes (**Figure 1a**). In situ ellipsometry studies with the flow cell shown in Figure 1b indicate that the layer thickness of PEM increased linearly similar to SPR studies. Moreover, ellipsometry data show that equilibrium adsorption states of polyelectrolytes were reached rather quickly. The overall thickness of multilayers at dry condition was ~8.9 nm (**Figure S1**), while that at wet condition

was ~18 nm (see **Figure 1b**). The growth of multilayers studied by SPR and ellipsometry expressed a linear behavior as it has been observed for similar multilayer systems made of Chi and HA [36].

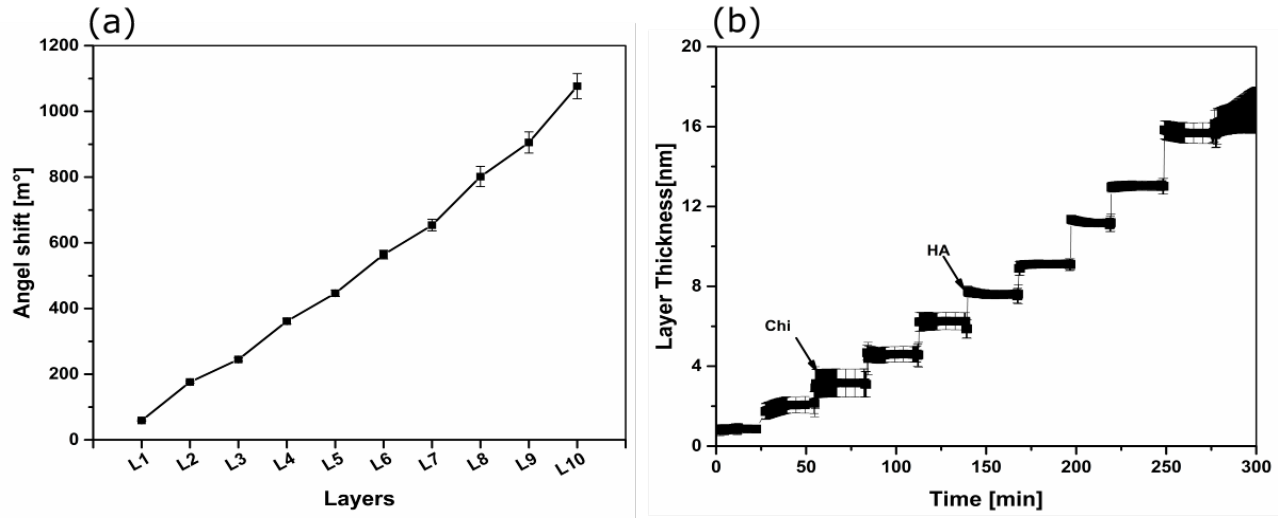

Figure 1: Multilayer growth and thickness. (a) angle shifts during multilayer formation measured with surface plasmon resonance (SPR). Odd layers: polycation (Chi); even layers: polyanion (HA). Results represent means ± SD, n = 3. (b) In situ thickness measurement of PEM by ellipsometry at wet conditions. Results represent means ± SD, n = 3.

Multilayers were then exposed to solutions of metal ions to achieve intrinsic cross-linking by ionic interaction or complex formation between metal ions and functional groups of both polysaccharides. First, an elemental analysis was performed using ICP-MS to determine the quantity of incorporated metal ions. Here $[Chi/HA]_5$ were loaded with the highest concentration of metal ions, such as 50 mM of Ca^{2+}, Co^{2+}, Cu^{2+} and 10 mM of Fe^{3+} respectively. In general, concentrations of metal ions detected in $[Chi/HA]_5$ multilayers were rather low, which is important when judging a potential cytotoxicity of metal ions like Co^{2+} and Cu^{2+}. **Table 1** shows the highest concentration for Fe^{3+}, followed by Ca^{2+} and Cu^{2+} having one order of magnitude lower concentration and then Co^{2+} with two orders of magnitude lower concentration than Fe^{3+}. We expected a cross-linking process of functional groups of both polysaccharides, particularly amino and hydroxyl groups of Chi and functional groups of HA (hydroxyl groups and carboxylic

groups) by coordinative bond formation. Hence, the Lewis acid/base character of the metal ions and functional groups should be considered. While amino groups, hydroxyl groups and carboxylic groups represent strong Lewis bases [37,38], the metal ions applied here belong to different categories of Lewis acids. Iron and copper ions represent strong Lewis acids, cobalt is of intermediate strength, while calcium is a weak Lewis acid. Pairing of strong Lewis acids with strong bases leads to stronger coordinative bond formation than strong with weak, which may explain the differences in the quantities of metal ions found in the PEM [39,]. In addition, we should also consider Coulomb interactions between metal ions and charged functional groups of polysaccharides, which would also indicate that the valency of metal ions plays a role for the uptake by $[Chi/HA]_5$ multilayers. Hence, the highest concentration of iron can be explained by both the strong Lewis acid character and higher valency compared to the other metal ions. Also higher concentration of copper ions should be related to its property being a strong Lewis acid. On the other hand, calcium as weak Lewis acid should be characterized by lower concentration than cobalt ions, which was not the case. Hence, we expect that calcium ions cross-link carboxylic groups of HA by Coulomb interaction.

Table 1: Amounts of metal ions absorbed in $[Chi/HA]_5$ multilayers prepared on glass. Quantities of metal ions on multilayers were determined by ICP-MS.

Quantity of metal ions on multilayers (µM and ng/cm²)	**$[Chi\text{-}HA]_5Ca^{2+}$**	**$[Chi\text{-}HA]_5Co^{2+}$**	**$[Chi\text{-}HA]_5Cu^{2+}$**	**$[Chi\text{-}HA]_5Fe^{3+}$**
[µM]	0.37	0.013	0.1	19
[ng/cm²]	13.3	0.69	4.87	926

FTIR spectroscopy was used to investigate which functional groups of both polysaccharides were involved in either ionic or coordinative bond formation with metal ions. Hence spectra of pure chitosan (Chi), hyaluronic acid (HA), and $[Chi/HA]_{100}$ prepared as freestanding films were studied with FTIR spectroscopy (see supplemental information for details of freestanding film formation (**Figure S2**)). The multilayer system was then exposed to highest concentrations of metal ions and FTIR spectra were recorded. **Figure 2a** shows that the spectrum of pure Chi

presents a broad absorbance band at about 3275 cm^{-1} related to the corresponding amine N–H and hydroxyl group O–H, including those from residual water. Furthermore two bands at 2980 and 2881 cm^{-1} caused by stretching of C-H; the absorption band of amide I stretching at 1651 cm^{-1}, and bending vibrations of the N-H (N-acetylated residues, amide II band) at 1587 cm^{-1} were found [40]. Amine deformation vibrations usually produce strong bands in the range of 1638-1575 cm^{-1}. Hence, the peak at 1587 cm^{-1} can be also a contribution of the N-H bending of the amine, as previously discussed [41]. The peaks at 1419 and 1377 cm^{-1} belong to the deformation of C-H and the stretching of C-N, respectively [42-43]. The absortion bands at 1150 cm^{-1} (anti-symmetric stretching of the C-O-C bridge and C-N stretch), 1075 cm^{-1}, 1050 cm^{-1} and 1030 cm^{-1} (skeletal vibrations involving the C-O stretching) are characteristics of its saccharide structure [40, 41].

The spectrum of HA (see **Figure 2a** as well) shows an intense band that has its maximum at about 3275 cm^{-1} attributed to N-H and O-H groups engaged in hydrogen bond formation and some residual water after drying of free-standing films. The band at around 2900 cm^{-1} can be referred to stretching vibration of the C-H bonds. The carbonyl band $\nu_{C=O}$ of the (protonated) carboxylic group COOH appears at 1730 cm^{-1}; this group has also been assigned to the peak at 1608 cm^{-1} [44]. This zone is where amide I and amide II are expected and probably their contributions superpose, the peak at 1555 cm^{-1} attributed to the amide II vibration [45]. The bands at about 1400 cm^{-1} are also characteristic of hyaluronic acid and correspond to C=O and C-O bonds in the carboxylate[46]. The intense band extending between 1200 and 900 cm^{-1} corresponds to the saccharide unit C-O-C stretching vibration (1150 cm^{-1} O-bridge, 1070 cm^{-1} and 1024 cm^{-1} C-O vibration).

LbL assembly of $[Chi/HA]_{100}$ multilayer films was not expected to produce significant changes in the FTIR spectrum of the polysaccharides, as reported previously for alginate and chitosan [41]. The [Chi/HA] multilayers presented a slightly sharp peak of the stretching bonds of O-H and N-H at 3275 cm^{-1} that shifts to 3300 cm^{-1}; a small new band at 1317 cm^{-1} that can be attributed to C-O and C-N amid II bands. The bands at 1602 and 1404 cm^{-1} can be related to the stretching of COO^- of the acid group of HA molecules. The bands corresponding to the

saccharide units between 1200 and 900 cm^{-1} are very similar to those found in the HA spectrum [47]. Metal ions can be electrostatically bound to the multilayers by the carboxylic groups of HA (COO^-) and/or be involved as coordinative bonds with hydroxyl or carbonyl oxygen of both polysaccharides or nitrogen in amino groups of Chi [29]. FTIR spectra of multilayers after addition of metal ions were similar to that of $[Chi/HA]_{100}$ (**see Figure 2b**). While previous studies reported a decrease in the intensity of the wideband at 3300 cm^{-1} (O–H and N–H stretching) due to the participation of the hydroxyl and amine groups in the chelation with metal ions [48], in our case this band remains of the same intensity as $[Chi/HA]_{100}$ or has a higher intensity that becomes evident for $[Chi/HA]_{100}$-Cu^{2+}. The band at 1602 cm^{-1} seems similar to the case of $[Chi/HA]_{100}$ (**Figure 2c**), but a slight shift to a higher wavenumber is observed to 1605 cm^{-1} when Co^{2+} or Ca^{2+} were present and up to 1608 cm^{-1} for Fe^{3+} and Cu^{2+} (redshift)). These shifts can indicate the interaction between the carboxylic group (COO^-) of HA and the metal ions as reported previously [49]. A slight shift of the bands to higher wavelengths is also observed in metal ion-containing [Chi/HA] multilayers for the peaks at 1404 cm^{-1} to 1406 cm^{-1} for Co^{2+} and Cu^{2+} and to 1410 cm^{-1} for Ca^{2+} and Fe^{3+} (**Figure 2c**), probably also due to the interaction of metal ions with the carboxylate group. In general, the small changes of the IR spectra at a range of ~ 5 to 10 cm^{-1} indicate the involvement of the amino and carboxyl groups in the complex formation. A weaker intensity and slight movement to a higher wavenumber of the C-O glycosidic bond at 1070 cm^{-1} was observed for the iron and cobalt-containing samples (**Figure 2d**), which might be attributed to the coordination of ions with adjacent monomeric units [43, 48].

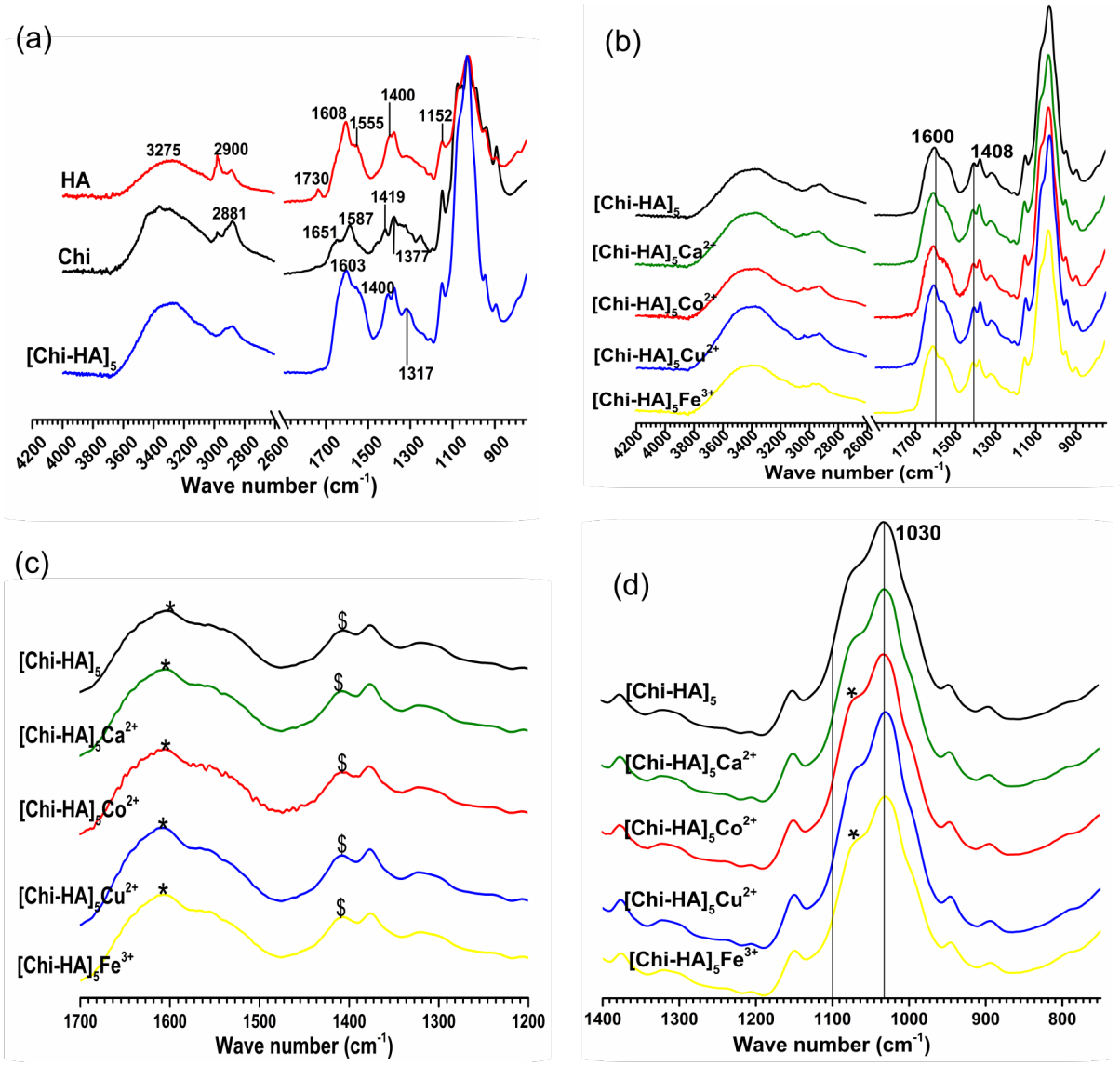

Figure 2: (a) FTIR spectra of pure chitosan (Chi), hyaluronic acid (HA) and dry $[Chi/HA]_{100}$ multilayer films. (b) FTIR spectra after cross-linking $[Chi/HA]_{100}$ with metal ions applying concentrations of 50 mM Ca^{2+}, Co^{2+}, Cu^{2+} and 10 mM of Fe^{3+}. (c) FTIR spectra after cross-linking $[Chi/HA]_{100}$ with metal ions in the range of 1600-1400 cm^{-1}, (*, $ indicate slight changes of spectra). (d) FTIR spectra after cross-linking $[Chi/HA]_{100}$ with metal ions in the range of 1100-1030 cm^{-1}.

3.2. Characterization of surface properties

Surface energy (wettability), which is dependent on the chemical composition of substrata, has an impact on cell spreading and growth [50]. Static water contact angle (WCA) measurement is one of the most suitable methods for measure the wettability. The captive bubble technique was used here to evaluate the changes of wetting properties of terminal layers and after absorption of metal ions by the multilayers. **Figure 3a** shows the original $[Chi/HA]_5$ multilayer as moderately wettable surfaces with WCAs in the range of 40 °C, which corresponds well to previous studies [31]. HA that forms the terminal layer possesses polar hydroxyl and negatively charged carboxylic groups. Hence, it forms a wettable material surface [51] .The treatment of $[Chi/HA]_5$ with the different metal ions resulted in slight changes of WCA. There were no significant changes in wettability as a result of adsorption of Cu^{2+} and Fe^{3+} ions of different concentrations compared to $[Chi/HA]_5$ multilayer. By contrast, a significant decrease of WCA was observed at higher concentrations of cobalt and calcium ions cross-linking to $[Chi/HA]_5$. This increase in surface wettability presented by a water contact angle of 30° ± 5° of $[Chi/HA]_5$ Ca^{2+} and Co^{2+}cross-linking, could be related to the entrapment of water in the $[Chi/HA]_5$ multilayers, as found in another study [52]. However, it should be noted that the metal ions only slightly influenced wetting properties of original $[Chi/HA]_5$. In addition, there was no correlation between quantities of metal ions taken up as found by ICP-MS since Fe^{3+} concentration was highest, but no change of WCA was seen.

Zeta potential measurements of PEM represent not only the charge distribution of terminal layers but also the electrical potential of the swollen layers beneath, which is in contrast to WCA measurements, where wettability is controlled only by the terminal layer composition [53]. In general, the zeta potentials of PEM reflect their intermingled structure in the surface region, at least when polysaccharides are used. Therefore, the polycations dominate the surface potential at acidic pH values, while polyanions dominate at basic pH values [54]. It was expected that addition of metal ions could change surface potentials by cross-linking carboxylic groups of HA due to ionic interaction or the presence of cationic metal ions. **Figure 3b** shows that the

zeta potentials of original $[Chi/HA]_5$ multilayers and those cross-linked with Cu^{2+} and Co^{2+} did not differ significantly particularly at acidic pH from the original $[Chi/HA]_5$, which corresponds well to the fact that their concentrations were really low as found by ICP-MS studies. Therefore it was expected that they have only a small effect. However, the zeta potentials of $[Chi/HA]_5$ cross-linked with Ca^{2+} and Fe^{3+} ions became more positive at acidic pH values, with most positive value when Ca^{2+} ions were used, which could be related to the interaction of calcium with carboxylic groups of HA due to ionic interaction. Corresponding to that observation, the point of zero charges (PZC) was found at pH 4.2 of $[Chi/HA]_5$ cross-linked with metal ions like Co^{2+}, Cu^{2+}, which was the same as for the original multilayer. A slight shift to 4.6 was seen when Fe^{3+} was applied, while that of $[Chi/HA]_5$-Ca^{2+} was found at pH 5.8. The more positive potentials and shift of PZC to higher pH values when Ca^{2+} and Fe^{3+} were used indicates that Coulomb interaction of cations with carboxylic groups of HA plays a dominate role and leads to a reduction of negative charge. In addition, also the higher concentration of them can add on, when they are involved in coordinative bond formation only since their cation charge remains then [55]. At physiological pH 7.4, original $[Chi/HA]_5$ and metal ions cross-linking exhibited similar negative zeta potentials.

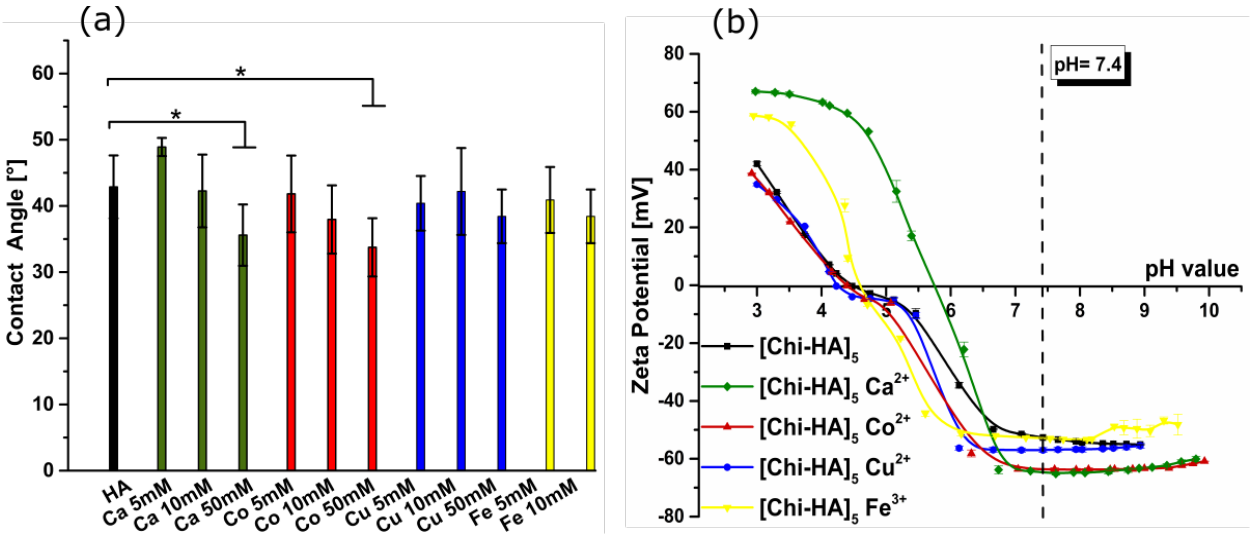

Figure 3: Water contact angles (WCAs) and zeta potential of multilayers. (a) Captive-bubble technique measuring WCA of plain (HA) and $[Chi/HA]_5$ multilayers cross-linked with metal ions. Results represent means ± SD (n = 15, *p < 0.05). (b) Zeta potentials of plain (black) and

$[Chi/HA]_5$ multilayers cross-linked with metal ions at higher concentration green Ca^{2+}, red Co^{2+}, blue Cu^{2+} (50 mM) and yellow Fe^{3+} (10 mM). All samples were measured twice (n = 2).

The surface topography of multilayer films was studied under ambient conditions in dry state with AFM. **Figure 4a** illustrates that the topography of original $[Chi/HA]_5$ multilayers and cross-linked with metal ions did not show significant differences between the type of metal ions except when Fe^{3+} was used for cross-linking. All surfaces had a granular surface morphology with slight differences in roughness depending on the type of metal ion (see **Table 2**). The $[Chi/HA]_5$ multilayer possessed a smoother surface (sq = 4.4 nm), while a granular structure of PEM led to increasing surface roughness after cross-linking with Cu^{2+} and Co^{2+}, but no effect for Ca^{2+}. By contrast, the $[Chi/HA]_5$-Fe^{3+} multilayers exhibited a less granular topography and more homogeneous structure but of highest roughness (sq = 11.7 nm). The Young's modulus (*E*) can be used to characterize the mechanical properties of $[Chi/HA]_5$, which tend to have elastic modulus values ranging from MPa to GPa. This is assumed also to reflect the solid substratum underneath [56]. It was expected that cross-linking of carboxyl and amino groups from HA and Chi by metal ions should increase the E modulus. By contrast, the E modulus distribution graphs shown in **Figure 4b** and mean values shown in (**Table 2**) demonstrate that the original $[Chi/HA]_5$ possessed the highest modulus while cross-linked with metal ions lead to lowering of Young's modulus in all cases. The cross-linking of $[Chi/HA]_5$ multilayers with Co^{2+} resulted in the lowest E modulus with the most narrow peak. However, also the other metal ions caused similar effects, but with wider distribution of the E moduli. We assume that rather intramolecular than intermolecular cross-linking of functional groups is causing a more coiled conformation of polyelectrolytes molecules inside the PEM leading to a reduction of elastic modulus as found also in other studies [57] [58].

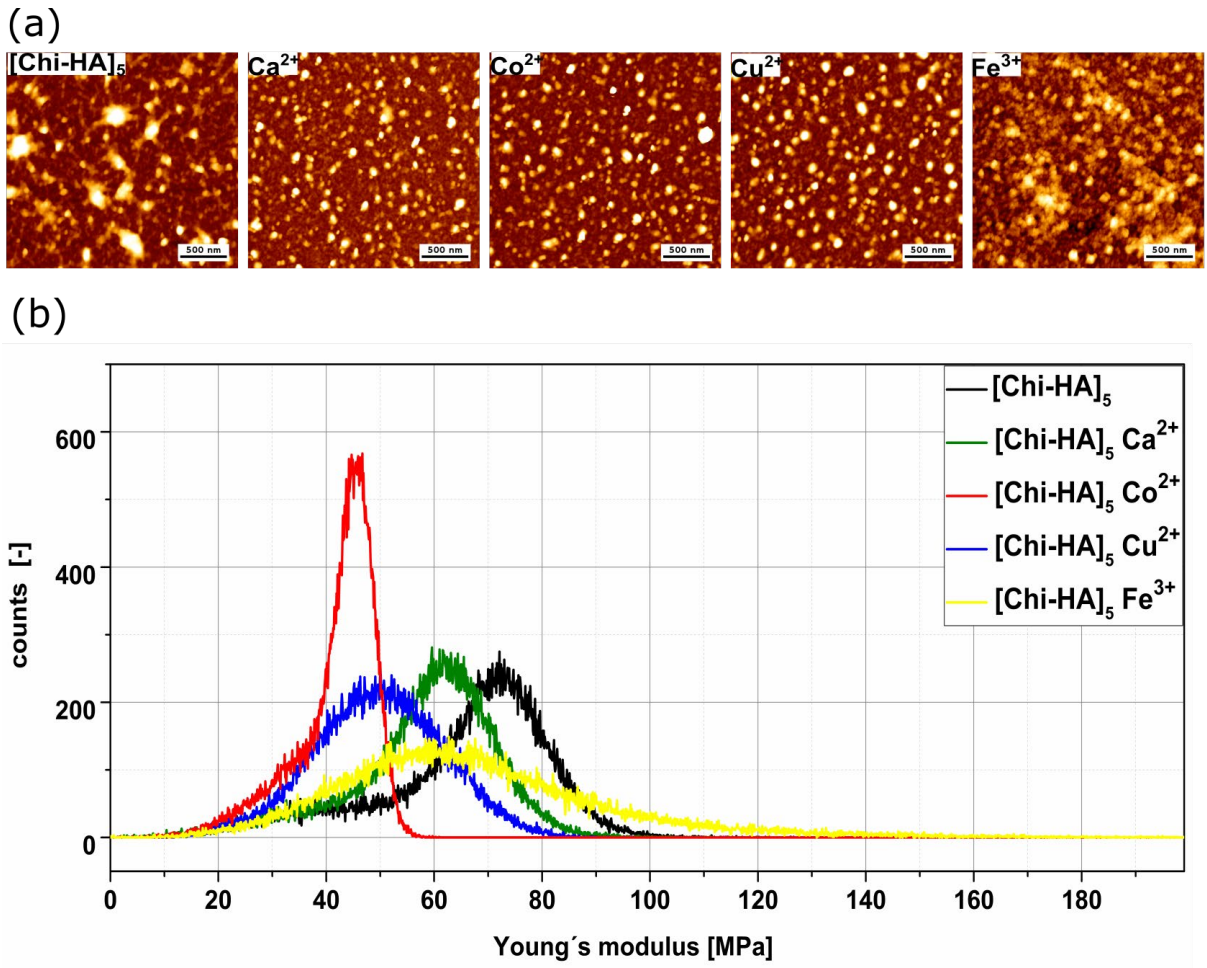

514

515 **Figure 4:** (a) Surface topography of $[Chi/HA]_5$ multilayers cross-linked with highest
516 concentrations 50 mM Ca^{2+}, Co^{2+}, Cu^{2+} and 10 mM Fe^{3+} measured under dry conditions by
517 atomic force microscopy (AFM). (b) Distribution curves of E modulus done at intermittent
518 contact mode of AFM in 150 mM NaCl solution with a force map of an area of 2.5 x 2.5 μm^2
519 (scale bar = 500 nm).

Table 2: Area roughness parameters (area mean roughness **(Sa)** and area root mean squared roughness), the elastic modulus (E) distribution of original $[Chi/HA]_5$ and with high concentration of metal ions were measured by AFM.

	$[Chi\text{-}HA]_5$	**Ca^{2+}**	**Co^{2+}**	**Cu^{2+}**	**Fe^{2+}**
Sq[a] [nm]	4.4	4.9	6.5	5.3	11.7
Sa[b] [nm]	2.8	2.7	4.2	3.4	7.9
E modulus (MPa)	71.3 ± 0.06	61.6 ± 0.05	45 ± 0.03	49.9 ± 0.03	62 ± 0.08

3.3. *Biological studies on serum protein adsorption and cell adhesion*

Since proteins are important mediators for cell-biomaterial interactions, the capability of $[Chi/HA]_5$ multilayers to bind proteins from a solution of 10% FBS was investigated using a standard BCA assay. The adsorption of serum proteins from FBS was dependent on type and concentration of metal ions. **Figure 5** shows that significantly more proteins adsorbed on $[Chi/HA]_5$-Cu^{2+} and $[Chi/HA]_5$-Fe^{3+} of highest concentration (50 and 10 mM, respectively) compared to $[Chi/HA]_5$. By contrast, cross-linking of $[Chi/HA]_5$ with calcium and cobalt ions had no significant effects on protein adsorption. The stronger adsorption of serum proteins observed when 10 mM Fe^{3+} were used for cross-linking might be related to the higher quantities of Fe^{3+} ions bound to multilayers and their effect on zeta potential because protein adsorption depends also on electrostatic interactions between the proteins and surfaces [59] [60]. Also the use of copper ions for the cross-linking increased the measured amount of serum proteins. On the other hand, there were no effects observed when Ca^{2+} and Co^{2+} were used for the cross-linking of $[Chi/HA]_5$ multilayers.

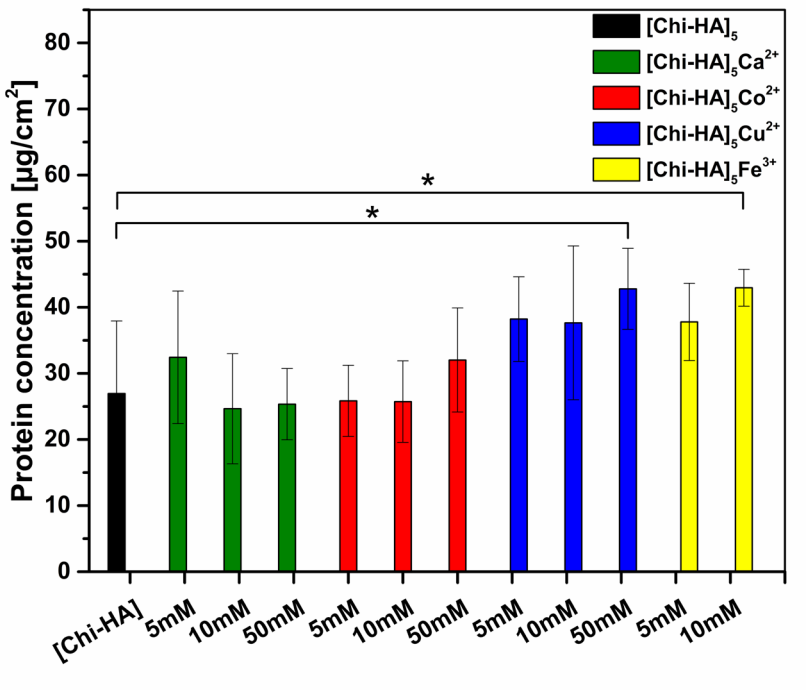

Figure 5: Measurement of adsorbed serum proteins on $[Chi/HA]_5$ multilayers (black) in dependence on the concentration of metal ions (green) Ca^{2+}, (red) Co^{2+}, (blue) Cu^{2+}, and (yellow) Fe^3 used for cross-linking determined by BCA assay (n = 6, *p < 0.05).

C3H10T1/2 fibroblasts stained for actin cytoskeleton were used for quantitative analysis of cell adhesion after 4 h on plain and metal ion cross-linked $[Chi/HA]_5$ multilayers including cell count, cell area, and aspect ratio. Results are shown in **Figure 6**. A first finding was that increasing metal ions concentration of Co^{2+} and Cu^{2+} caused a significant decrease in cell count (**Figure 6a**). However, no significant effects were seen regarding cell count for Fe^{3+} and Ca^{2+} compared to original $[Chi/HA]_5$ multilayers independent on the concentration of metal ions used for cross-linking. On the other hand, effects of cross-linking $[Chi/HA]_5$ multilayers with metal ions on cell spreading (**Figure 6b**) were visible already at low concentrations (5 mM) of iron resulting in the largest area of cells. Besides, the cell area was not significantly different between the plain $[Chi/HA]_5$ and those cross-linked with Ca^{2+}, Co^{2+} and Cu^{2+} at a low concentration of 5 mM. However, higher concentrations of all ions from 10 mM on made all cells significantly larger than those on plain $[Chi/HA]_5$ multilayers. Furthermore, **Figure 6c** shows that cells were significantly more polarized on $[Chi/HA]_5$ cross-linked with copper (10 and 50 mM) and iron (5 and 10 mM) ions than cells on $[Chi/HA]_5$. By contrast, cross-linking of $[Chi/HA]_5$ with calcium and cobalt ions did not have any significant effects on cell shape if compared to plain $[Chi/HA]_5$ as visible by comparable aspect ratioa (Figure 6c).

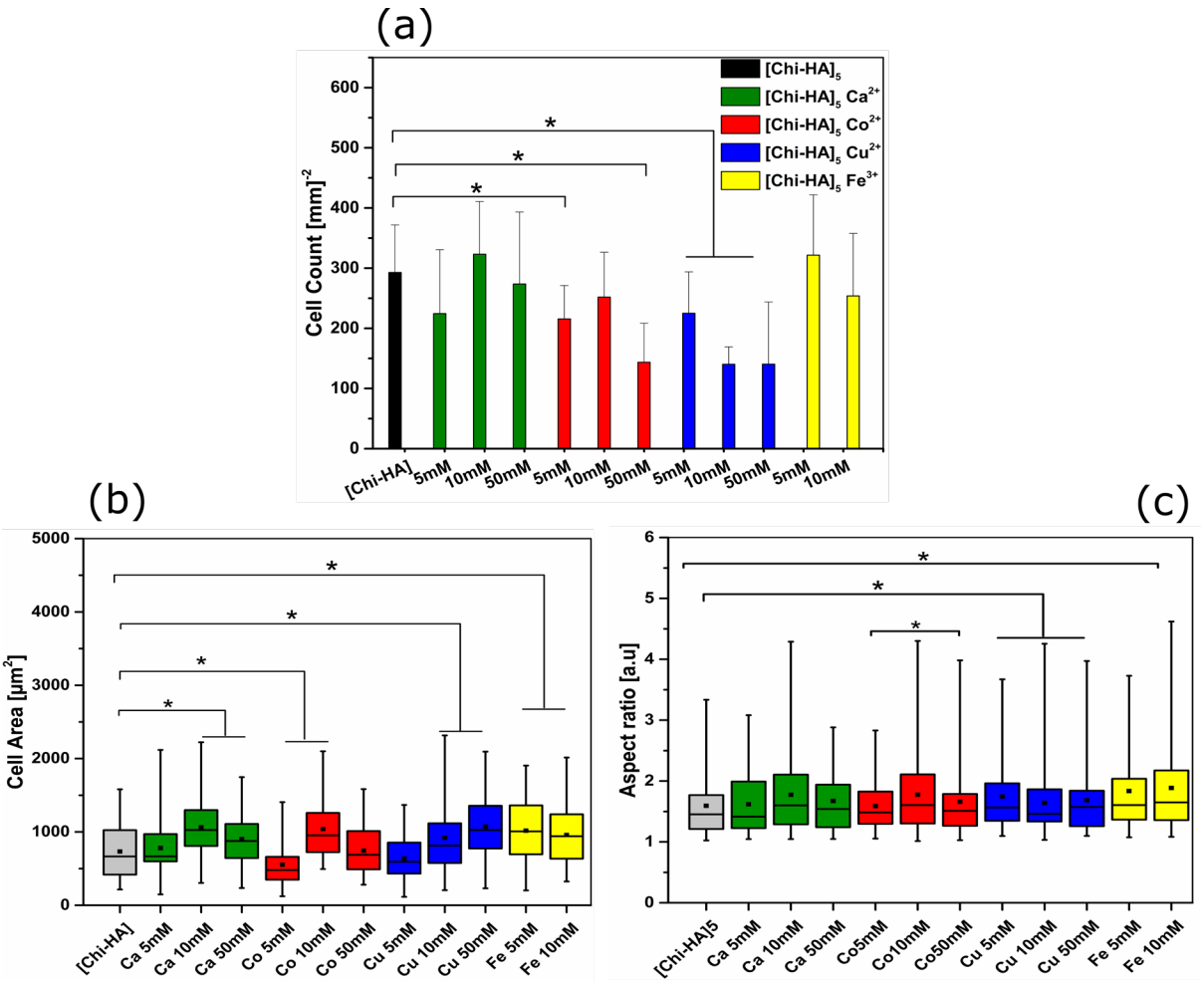

Figure 6: Quantitative cell adhesion data obtained from CLSM micrographs of C3H10T1/2 embryonic fibroblasts cultured for 4 h on the different types of multilayers in medium with 10% FBS. Cell count (a), area (b), and aspect ratio (c) of cells on original $[Chi/HA]_5$ and cross-linked with different metal ions concentrations. The box-whisker plots in panels (b) and (c) indicate the 25th and 75th percentile, the median and mean values (black square), respectively (mean ± SD).

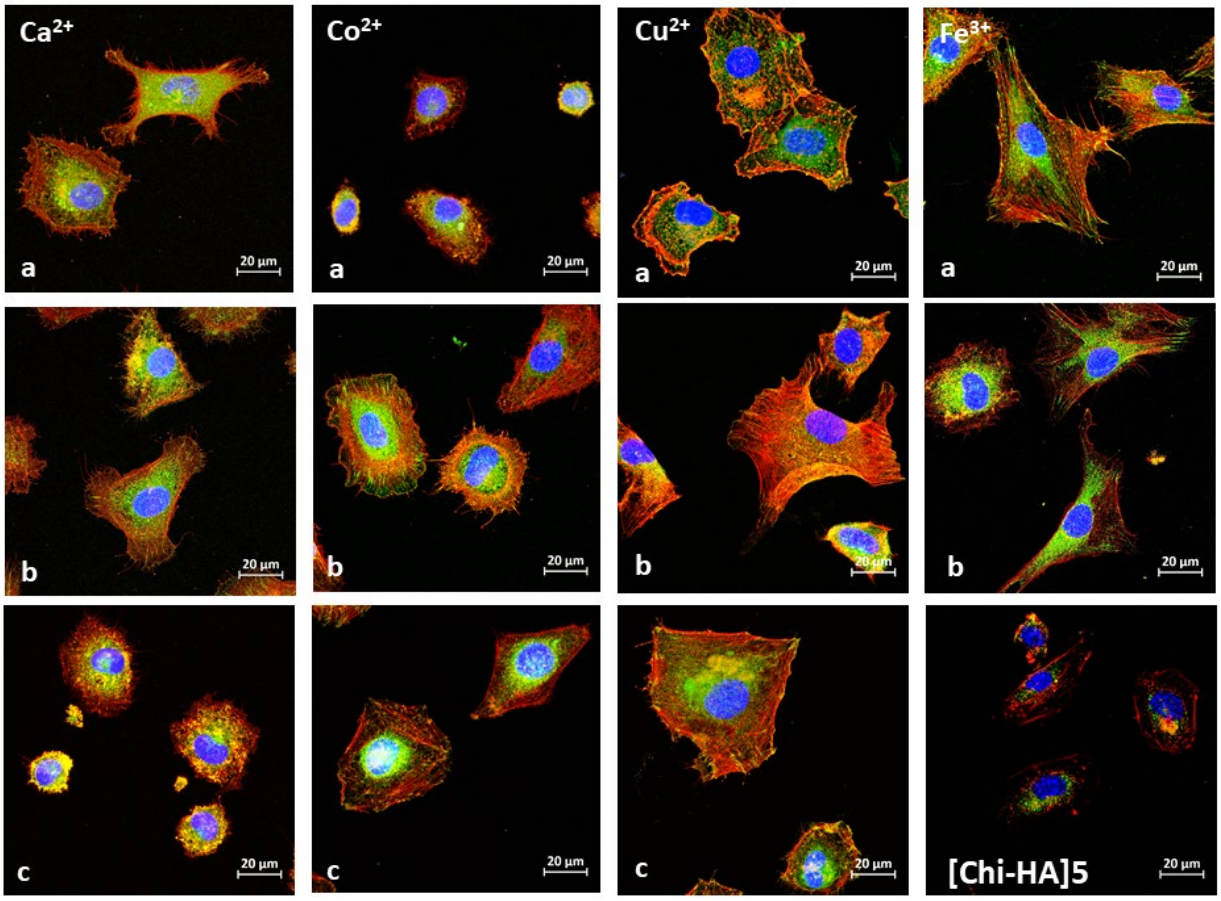

Figure 7: Cell morphology of C3H10T1/2 embryonic fibroblasts after 4 h incubation on $[Chi/HA]_5$ and multilayers cross-linked with metal ions of concentration of 5 (a), 10 (b) and 50 mM (c), respectively. Cells were stained for actin filaments (red), vinculin (green) and nuclei (blue). (Scale bar: 20 µm)

Immunohistochemical staining of C3H10T1/2 embryonic fibroblast was used to study cell adhesion and spreading through staining of actin cytoskeleton (red) expression and organization of vinculin (green) to detect focal adhesion (FA) formation and cell nuclei (blue) using CLSM (**Figure 7**). C3H10T1/2 cells plated on plain $[Chi/HA]_5$ exhibited a poor expression of vinculin and no organization in focal adhesion plaques (FA), which corresponds probably to the lack of appropriate matrix ligands for cellular integrins (e.g. fibronectin). Although the expression of vinculin seemed to be stronger in cells plated on $[Chi/HA]_5$ cross-linked with Ca^{2+} and Co^{2+} development of FA was not seen. By contrast, already 5 mM Fe^{3+} led to more elongated cells that possessed many well-developed FA that was also corresponding to the

presence of many longitudinal actin stress fibers, not seen with the other metal ions used at the same concentration for the cross-linking process. Whereas, the $[Chi/HA]_5$ multilayers cross-linked with 10 mM of all metal ions promoted formation of FA in cells, seen at the periphery and in the central regions accompanied by development of actin stress fibers. However, a further increase of metal ion concentration to 50 mM during the cross-linking process caused not only a reduction of cell size, but also to a disappearance of focal adhesions when Ca^{2+} and Co^{2+} were used for cross-linking.

CD44 is a mediator for HA-induced cell adhesion and signaling pathways[13]. Here, we examined whether CD44 was expressed and organized differently (green staining) in dependence of the type of metal ion used for cross-linking. In addition, actin (red) and nuclear staining (blue) were performed to visualize nuclei and the body of cells (**Figure 8a**). CD44 staining was predominantly distributed perinuclear manner as indicated by the green background around the blue-stained nuclei of cells. However, positive CD44 staining in the peripheral regions of cells cultured on $[Chi/HA]_5$ cross-linked with metal ions was also found as clusters in the periphery and not seen in cells on the plain PEM. Such clustered appearance of CD44 was detected on both $[Chi/HA]_5$-Co^{2+} and -Cu^{2+}, which expressed additionally a strong CD44-positive staining in the nucleus of permealized cells. A weak positive staining for CD44 in the nucleus was also observed in cell cultured on plain $[Chi/HA]_5$. A quantitative analysis of these results studied by the intensity ratio nuclei to the cytoplasm of CD44 using the Fiji ImageJ confirmed the visual observations in a manner showing that both ions copper and cobalt provoked stronger nuclear staining of CD44 (**Figure 8b**).

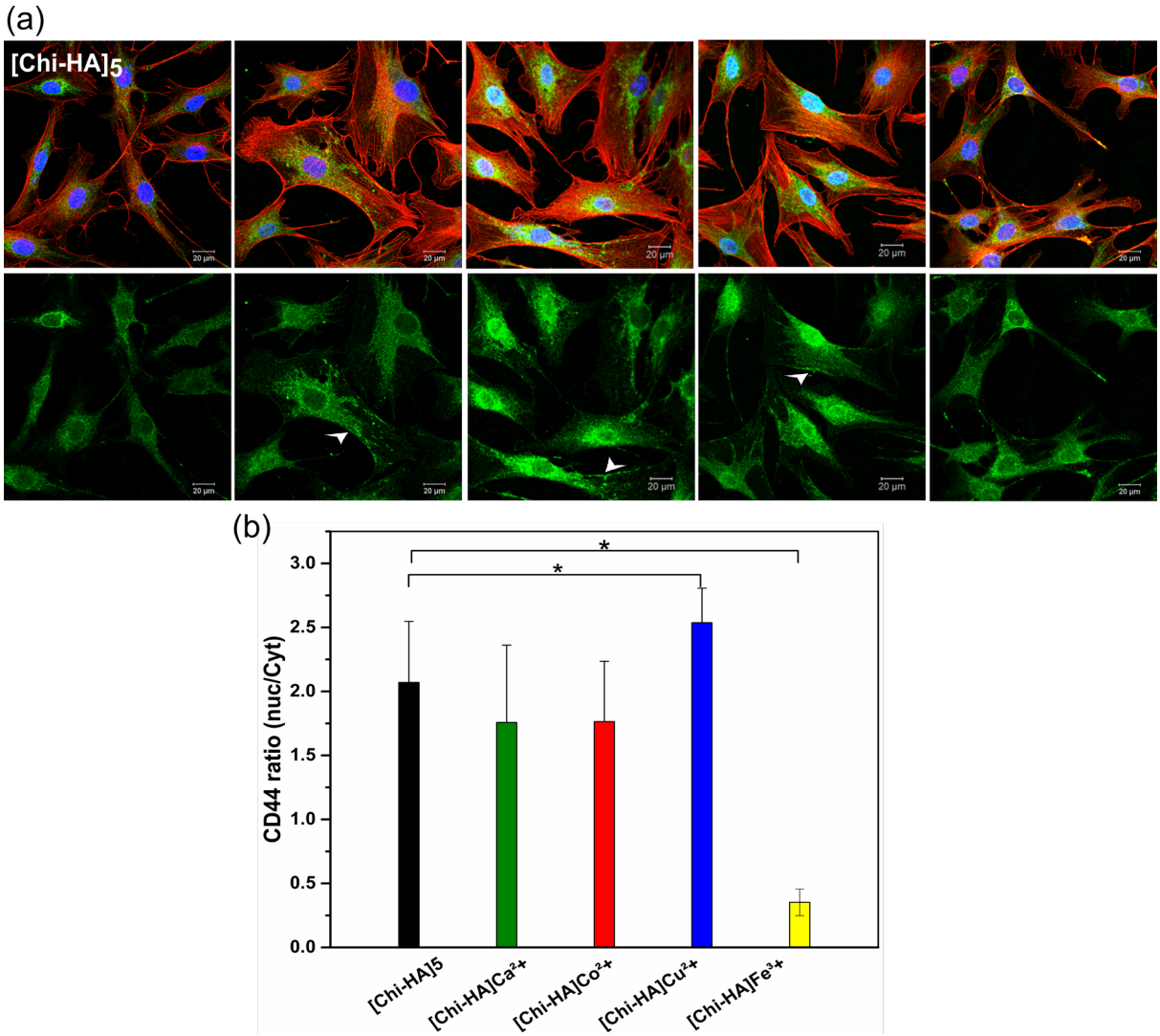

598

599 **Figure 8:** (a) Scanning confocal micrographs of cells, which were stained for actin filaments
600 (red), CD44 (green) and nuclei (blue) in upper lane and of CD44 only (lower lane), and (b)
601 intensity ratio nuclei to cytoplasmic staining of CD44 in C3H10T1/2 embryonic fibroblasts after
602 24 h incubation on plain and with 50 mM Ca^{2+}, Co^{2+}, Cu^{2+} or 10 mM Fe^{3+} cross-linked $[Chi/HA]_5$
603 multilayers. White arrows in the micrographs indicate peripheral cell areas of increased CD44
604 expression. For quantification of intensity ratio Fiji ImageJ was used.

605

606 The results of adhesion experiments show that cross-linking $[Chi/HA]_5$ multilayers with Cu^{2+}
607 and Fe^{3+} promote adhesion, particularly spreading and partly polarization of C3H10T1/2
608 fibroblasts, while Ca^{2+} and Co^{2+} seem to be inhibitory, particularly when 50 mM of salt ions
609 were used. The inhibitory effect of the latter seems to be related to the fact that with increasing

concentrations of both metal ions, wettability of $[Chi/HA]_5$ multilayers was increased, which is suppressing cell adhesion [50] . Moreover, measurements of E modulus revealed that the cross-linking with Co^{2+} resulted in the softest surface, which may be also related to lower spreading of cells [18]. In addition, there was also no promoting effect of cross-linking $[Chi/HA]_5$ multilayers with Ca^{2+} and Co^{2+} on serum protein adsorption, which represents a prerequisite for cell adhesion to bind attachment factors like vitronectin from serum that promote integrin ligation in cells [12]. This was obviously the case for multilayers cross-linked with Cu^{2+} and Fe^{3+}, both which promoted serum protein adsorption and showed enhanced cell spreading with increase of metal ion concentration. Increased attachment and spreading of cells on surfaces cross-linked with iron ions has been observed previously when chitosan films were exposed to the metal ion [61]. It was also interesting to see that CD44 could be found inside the nuclei when cobalt and copper ions were used for the cross-linking process. This points to a translocation of CD44, which has been related to changed transcription of genes in cells [62].

Cell growth requires adhesion of cells with ligation of integrins to ECM to stimulate signal transduction via the mitogen-activated protein (MAP) kinase and other pathways including signaling via CD44 upon binding of HA [13 63]. The growth of C3H10T1/2 cells was studied on the plain and cross-linked $[Chi/HA]_5$ multilayer after 24 and 72 h. Quantification of viable cells was done by Q Blue test that is equivalent to the quantity of metabolic active cells and is shown in **Figure 9a** and b (24 and 72 h). In addition, phase contrast images of cells grown for 24 h are shown in **Figure 9c**. The quantitative measurement of cell growth shows that the number of cells increased on $[Chi/HA]_5$ during the time of culture. Micrographs in **Figure 9c** show that cells formed almost confluent layers on $[Chi/HA]_5$ after 24 h. The use of calcium ions for cross-linking $[Chi/HA]_5$ multilayers had an inhibitory and concentration-dependent effect on quantity of cells measured by Q Blue after 24 h and showed also a significantly lower quantity of cells after 72 h if compared to $[Chi/HA]_5$. The morphology of cells shown in the micrographs taken after 24 h (see **Figure 9c**) demonstrate that the use of calcium ions for cross-linking lead to a rather round cell morphology and formation of cell aggregates in comparison to the

637 flat, spread phenotype of cells on $[Chi/HA]_5$. There were no effects of Ca^{2+} concentration visi-
638 ble here. The use of cobalt ions for cross-linking had also an inhibitory effect on the quantity
639 of cells measured with Q Blue assay after 24 h when compared to $[Chi/HA]_5$. However, it was
640 seen that higher concentrations of 50 mM Co^{2+} used during cross-linking of $[Chi/HA]_5$ were
641 related to a higher quantity of cells and this effect became stronger after 72 h. Micrographs
642 shown in **Figure 9c** support this finding because lower concentrations of Co^{2+} (5 and 10 mM)
643 were related to the formation of cell aggregates and low number of spread cells, while a higher
644 concentration of 50 mM Co^{2+} promoted spreading and increased growth of cells, particularly
645 visible after 72 h (see **Figure 9b**). In general, the use of calcium and cobalt ions for cross-
646 linking exhibited the lowest growth of cells, which fits well to the results of adhesion studies.
647 $[Chi/HA]_5$-Cu^{2+} multilayers showed a comparable quantity of cells measured by Q Blue assay
648 when compared to the original $[Chi/HA]_5$ multilayer with no effect of Cu^{2+} concentration after
649 24 h while after 72 h the number of cells was lower than on the $[Chi/HA]_5$ multilayer, but de-
650 creased slightly with increase in Cu^{2+} concentration from 5 to 50 mM. Micrographs show that
651 cells had a spread phenotype already at low concentration of 5 mM Cu^{2+} that was not changing
652 with increasing concentration (see **Figure 9c**). The use of Fe^{3+} for cross-linking $[Chi/HA]_5$ mul-
653 tilayers was clearly promoting cell growth and spread phenotype of cells already at low con-
654 centration of 5 mM (**Figure 9**). Cell quantity measured with Q Blue assays detected also more
655 cells than on the control $[Chi/HA]_5$ multilayers after 24 h and comparable quantities after 72 h
656 (**Figure 9 a, b**). The C3H10T1/2 cells were already growing to confluence after 24 h, when 10
657 mM Fe^{3+} was used for cross-linking as visible in **Figure 9c**. Findings regarding the growth of
658 of C3H10T1/2 cells on multilayers cross-linked with Cu^{2+} and Fe^{3+} fit also very well to the
659 observation made during adhesion studies because cell spreading is related to ligation of in-
660 tegrins and signal transduction processes [12]. Beside changes of physical surface properties
661 that are caused by the cross-linking of functional groups of both hyaluronan and chitosan,
662 specific effects of metal ions on cell behavior can be anticipated [64]. It should be also underlined
663 that the suppressive effects of calcium and cobalt ions used fo cross-linking are not due to

cytotoxic effects. We studied the effect of salt solutions in relevant contractions ranges in separate experiments on plastic-adherent cultures of C3H10T1/2 cells and did not find any signs of cytotoxicity (see **Figure S3).**

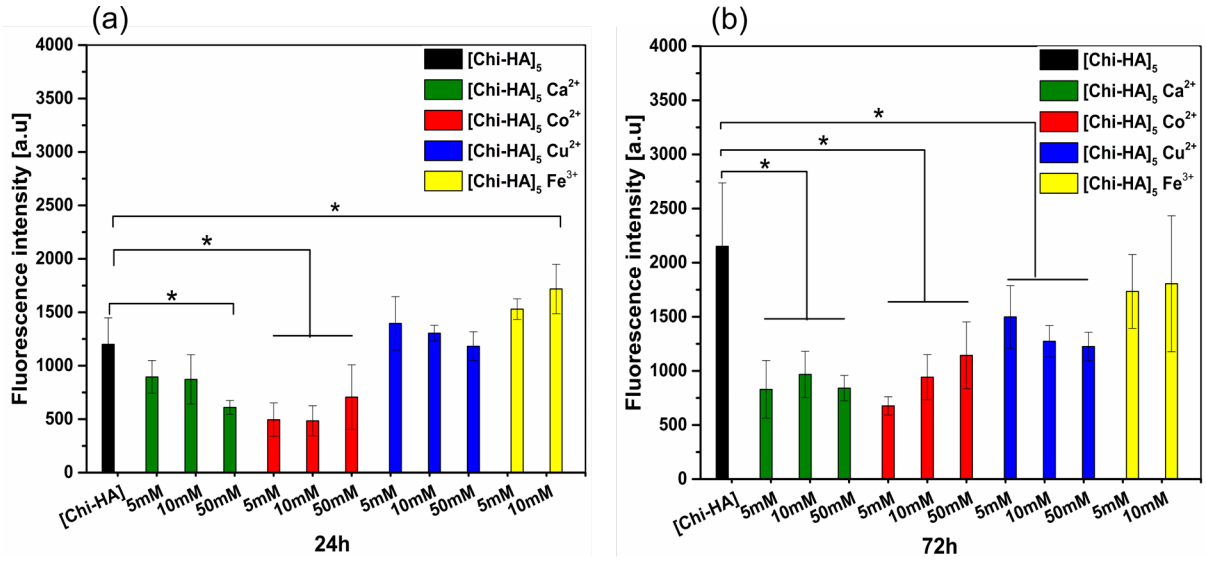

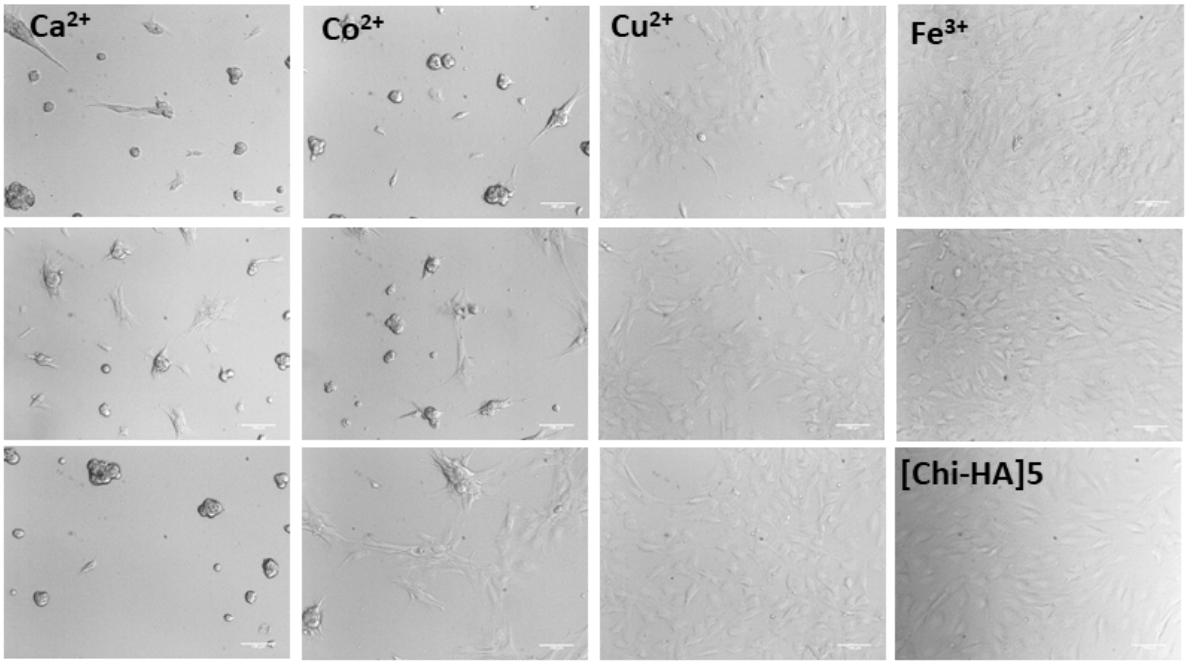

Figure 9: Proliferation of C3H10T1/2 cells plated on original [Chi/HA]$_5$ and cross-linked with metal ions. The metabolic activity was determined by the Q Blue viability assay 24 h (a) and 72 h (b) of culture. Results represent means ± SD of three independent experiments. (c) phase contrast images of C3H10T1/2 cells cultured in the presence of 10% FBS for 24 h on plain

673 $[Chi/HA]_5$ and cross-linked with metal ions of concentration of 5 mM: upper panel, 10 mM:
674 middle panel and 50 mM: lower panel of $[Chi/HA]_5$-Ca^{2+}, -Co^{2+}, -Cu^{2+} and -Fe^{3+}, respectively.

675 The effect of cross-linking $[Chi/HA]_5$ multilayers with metal ions was studied on adipogenic
676 differentiation of the multipotent mouse cell line C3H10T1/2 by histochemistry (oil red staining
677 of lipid vacuoles) and immunohistochemistry (perilipin and GLUT4) was studied after 21 days
678 of culture in normal culture medium (DMEM, 10% FBS and 1% Pen/strep) without any induc-
679 ers. **Figure 10a** shows positive staining of vacuoles with oil red when they were grown on
680 $[Chi/HA]_5$ multilayers cross-linked with Ca^{2+}, Cu^{2+} and Fe^{3+}, However, plain $[Chi/HA]_5$ and Co^{2+}
681 cross-linked multilayers did not show any presence of lipid vacuoles. Indeed, the strongest
682 staining was found when Cu^{2+} was used for cross-linking. Immunohistochemical staining of
683 perilipin and GLUT4 also confirmed absence of adipogenesis by lack or weak staining for both
684 markers of cells cultured on the plain and Co^{2+} cross-linked multilayers. This is in line with
685 previous findings that cobalt ions cause a suppression of the expression of adipogenic mark-
686 ers like PPARγ and inhibit adipogenesis as found by Kim et al. [65]. By contrast, the plain
687 $[Chi/HA]_5$ multilayers inhibited lipid accumulation in the cells, which corresponds to the fact
688 cells require inducers to differentiate [66], which lacks obviously during their culture on the plain
689 multilayers. By contrast, cells cultured on $[Chi/HA_]_5$- Cu^{2+} and Fe^{3+} showed strong expression
690 of perilipin and GLUT4 with the presence of many small vacuoles. Furthermore, it was also
691 observes that F-actin was weakly expressed in cells that were rich in vacuoles. The ATP7A
692 transporter protein is regulating copper ion uptake, which promotes adipogenic differentiation.
693 Hence, the expression of perilipin and GLUT4 in cells cultured on $[Chi/HA]_5$-Cu^{2+} is showing
694 upregulated adipocyte differentiation [67]. The previous study is also related to the important role
695 of iron-related genes such as IRP1 in adipocyte physiology [68], because also $[Chi/HA]_5$-Fe^{3+}
696 multilayers promoted adipogenesis. Another interesting finding was that C3H10T1/2 cells
697 tended to form aggregates when cultured on $[Chi/HA]_5$-Ca^{2+} and were positively stained for
698 lipids (see **Figure 10a**), as well as being positively-stained for perilipin. Calcium ions are
699 known to be involved in regulating and stimulating adipogenic differentiation through (PPAR

ɣ) receptor and cAMP [69]. In general, the peroxisome proliferator-activated receptor ɣ (PPAR ɣ), is a key transcription factor to regulate adipocyte maturation. Furthermore, overexpression of (PPAR ɣ) can produce a rounded morphology as seen in **Figure 10b**.

The findings on adipogenic differentiation of C3H10T1/2 cells cannot be explained simply by the physical effects of surfaces that are related to the different attachment and spreading of cells. Findings of McBeath at al. demonstrated that the spreading of mesenchymal stem cells is related to osteogenic differentiation, while a round phenotype of cells promotes adipogenesis[70]. Here, the more spread phenotypes found on $[Chi/HA]_{5v}$multilayers cross-linked with copper and iron ions promote adipogenic differentiation. Hence, we assume that release from or presentation of metal ions by the multilayers is the key to the differentiation of cells, though the quantities of ions is very low, but obviously they are bioactive.

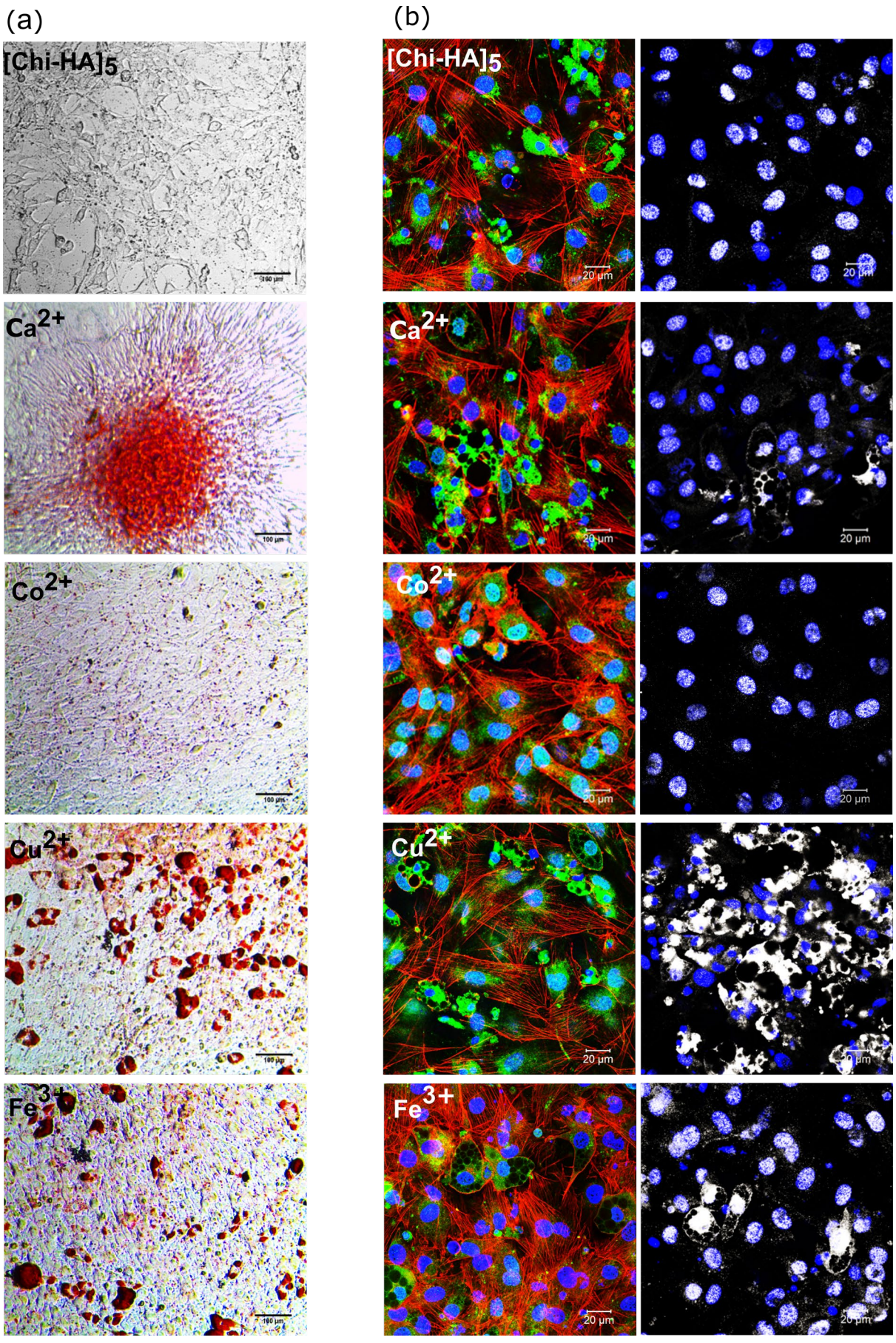
(a)
(b)
[Chi-HA]5
Ca2+
Co2+
Cu2+
Fe3+
100 µm
20 µm

Figure 10: Visualization of adipogenic differentiation, C3H10T1/2 cells grown for 21 days on plain and metal ion (highest concentration) cross-linked $[Chi/HA]_5$ multilayers. (a) Detection of lipid vacuoles formation using histochemical staining using oil red solution) (scale: 100 µm). (b) CLSM images of cell morphology by immunocytochemical staining for specific adipogenic differentiation markers. Cells were fixed with 4% paraformaldehyde and stained for perilipin (green) and (actin red) and the (nuclei blue) ((b) left lane). glucose transporter 4 (GLUT4, white) and the (nuclei blue) ((b) right lane) after 21 days incubation with DMEM (Scale: 20 µm).

4. Conclusions

In the present work, we studied the effect of cross-linking $[Chi/HA]_5$ multilayers with different types and concentrations of metal ions on bulk and surface properties of multilayers and how this affects the behavior of a multipotent mouse stem cell line. We found indications that cross-linking of $[Chi/HA]_5$ with metal ions multilayers can occur both through coordination chemistry but also Coulomb interaction, particularly for Ca^{2+} and Fe^{3+} with carboxylic groups of HA. Furthermore, an important observation of this study was that the different metal ions (type and concentration) only slightly affected surface properties such as topography and wettability of the original $[Chi/HA]_5$. In particular, it should be noted that low quantities of metal ions such as Cu^{2+} as shown by ICP-MS had considerable effects on cells behavior. Interestingly, $[Chi/HA]_5$-Ca^{2+}, -Cu^{2+} and -Fe^{3+} used at highest concentration for cross-linking promoted adipogenic differentiation of cells in the absence of any inducer media. Hence, we can show here for the first time that the combination of thin polyelectrolyte multilayers made of hyaluronan and chitosan cross-linked by metal ions can be used to control adhesion and differentiation of stem cells, which may pave the way for the use of such surface coatings without addition of cytokines for making bioactive implant materials.

Declaration of conflicting interests

The author(s) declare no potential conflicts of interest with respect to the research, authorship, and/or publication of this article.

Acknowledgements

This work was part of the High-Performance Center Chemical and Biosystems Technology Halle/Leipzig, supported by the European Regional Development Fund (ERDF), and a grant to HK from the Martin Luther University Halle-Wittenberg for female PhD students. The work was further supported by the Fraunhofer Internal Programs under Grant No. Attract 069-608203 (CEHS). TG acknowledges the kind support by the Ministry of Science and Higher Education of the Russian Federation within the framework of state support for the creation and development of World-Class Research Centers "Digital biodesign and personalized healthcare" 075-15-2020-926. GGF acknowledges funding by State Research Agency. Ministry of Science and Innovation of Spain, grant PID2019-106000RB-C21/AEI/10.13039/501100011033 project.

References

1. Castner, D. G.; Ratner, B. D., Biomedical surface science: Foundations to frontiers. *Surface Science* **2002,** *500* (1-3), 28-60.
2. Faucheux, N.; Schweiss, R.; Lützow, K.; Werner, C.; Groth, T., Self-assembled monolayers with different terminating groups as model substrates for cell adhesion studies. *Biomaterials* **2004,** *25* (14), 2721-2730.
3. Kofron, M. D.; Li, X.; Laurencin, C. T., Protein-and gene-based tissue engineering in bone repair. *Current opinion in biotechnology* **2004,** *15* (5), 399-405.
4. Fabbri, P.; Messori, M., Surface modification of polymers: chemical, physical, and biological routes. In *Modification of polymer properties*, Elsevier: 2017; pp 109-130.
5. Decher, G.; Hong, J. D.; Schmitt, J., Buildup of ultrathin multilayer films by a self-assembly process: III. Consecutively alternating adsorption of anionic and cationic polyelectrolytes on charged surfaces. *Thin solid films* **1992,** *210*, 831-835.
6. Clark, S. L.; Hammond, P. T., The role of secondary interactions in selective electrostatic multilayer deposition. *Langmuir* **2000,** *16* (26), 10206-10214.
7. Kotov, N., Layer-by-layer self-assembly: the contribution of hydrophobic interactions. *Nanostructured Materials* **1999,** *12* (5-8), 789-796.
8. Costa, R. R.; Mano, J. F., Polyelectrolyte multilayered assemblies in biomedical technologies. *Chemical Society Reviews* **2014,** *43* (10), 3453-3479.

9. Anouz, R.; Repanas, A.; Schwarz, E.; Groth, T., Novel surface coatings using oxidized glycosaminoglycans as delivery systems of bone morphogenetic protein 2 (BMP-2) for bone regeneration. *Macromolecular bioscience* **2018,** *18* (11), 1800283.
10. Guillame-Gentil, O.; Semenov, O.; Roca, A. S.; Groth, T.; Zahn, R.; Vörös, J.; Zenobi-Wong, M., Engineering the extracellular environment: strategies for building 2D and 3D cellular structures. *Advanced materials* **2010,** *22* (48), 5443-5462.
11. Hynes, R. O., The extracellular matrix: not just pretty fibrils. *Science* **2009,** *326* (5957), 1216-1219.
12. Hynes, R. O., Integrins: bidirectional, allosteric signaling machines. *cell* **2002,** *110* (6), 673-687.
13. Kim, Y.; Kumar, S., CD44-mediated adhesion to hyaluronic acid contributes to mechanosensing and invasive motility. *Molecular Cancer Research* **2014,** *12* (10), 1416-1429.
14. Bishop, J. R.; Schuksz, M.; Esko, J. D., Heparan sulphate proteoglycans fine-tune mammalian physiology. *Nature* **2007,** *446* (7139), 1030-1037.
15. Friedenstein, A. J.; Chailakhyan, R. K.; Latsinik, N. V.; Panasyuk, A. F.; Keiliss-Borok, I. V., Stromal cells responsible for transferring the microenvironment of the hemopoietic tissues: cloning in vitro and retransplantation in vivo. *Transplantation* **1974,** *17* (4), 331-340.
16. Barry, F. P.; Murphy, J. M., Mesenchymal stem cells: clinical applications and biological characterization. *The international journal of biochemistry & cell biology* **2004,** *36* (4), 568-584.
17. Dalby, M. J.; García, A. J.; Salmeron-Sanchez, M., Receptor control in mesenchymal stem cell engineering. *Nature Reviews Materials* **2018,** *3* (3), 1-14.
18. Engler, A. J.; Sen, S.; Sweeney, H. L.; Discher, D. E., Matrix elasticity directs stem cell lineage specification. *Cell* **2006,** *126* (4), 677-689.
19. Date, T.; Doiguchi, Y.; Nobuta, M.; Shindo, H., Bone morphogenetic protein-2 induces differentiation of multipotent C3H10T1/2 cells into osteoblasts, chondrocytes, and adipocytes in vivo and in vitro. *Journal of Orthopaedic Science* **2004,** *9* (5), 503-508.
20. Haas, K. L.; Franz, K. J., Application of metal coordination chemistry to explore and manipulate cell biology. *Chemical reviews* **2009,** *109* (10), 4921-4960.
21. Mourino, V.; Cattalini, J. P.; Boccaccini, A. R., Metallic ions as therapeutic agents in tissue engineering scaffolds: an overview of their biological applications and strategies for new developments. *Journal of the Royal Society Interface* **2012,** *9* (68), 401-419.
22. Glenske, K.; Donkiewicz, P.; Köwitsch, A.; Milosevic-Oljaca, N.; Rider, P.; Rofall, S.; Franke, J.; Jung, O.; Smeets, R.; Schnettler, R., Applications of metals for bone regeneration. *International journal of molecular sciences* **2018,** *19* (3), 826.
23. González-Vázquez, A.; Planell, J. A.; Engel, E., Extracellular calcium and CaSR drive osteoinduction in mesenchymal stromal cells. *Acta biomaterialia* **2014,** *10* (6), 2824-2833.
24. Wu, C.; Zhou, Y.; Fan, W.; Han, P.; Chang, J.; Yuen, J.; Zhang, M.; Xiao, Y., Hypoxia-mimicking mesoporous bioactive glass scaffolds with controllable cobalt ion release for bone tissue engineering. *Biomaterials* **2012,** *33* (7), 2076-2085.
25. Burghardt, I.; Lüthen, F.; Prinz, C.; Kreikemeyer, B.; Zietz, C.; Neumann, H.-G.; Rychly, J., A dual function of copper in designing regenerative implants. *Biomaterials* **2015,** *44*, 36-44.
26. Gérard, C.; Bordeleau, L.-J.; Barralet, J.; Doillon, C. J., The stimulation of angiogenesis and collagen deposition by copper. *Biomaterials* **2010,** *31* (5), 824-831.
27. Simovich, M. J.; Conrad, M. E.; Umbreit, J. N.; Moore, E. G.; Hainsworth, L. N.; Smith, H. K., Cellular location of proteins related to iron absorption and transport. *American journal of hematology* **2002,** *69* (3), 164-170.
28. Zheng, H.; Jiang, J.; Xu, S.; Liu, W.; Xie, Q.; Cai, X.; Zhang, J.; Liu, S.; Li, R., Nanoparticle-induced ferroptosis: detection methods, mechanisms and applications. *Nanoscale* **2021,** *13* (4), 2266-2285.

29. Mentbayeva, A.; Ospanova, A.; Tashmuhambetova, Z.; Sokolova, V.; Sukhishvili, S., Polymer–metal complexes in polyelectrolyte multilayer films as catalysts for oxidation of toluene. *Langmuir* **2012,** *28* (32), 11948-11955.
30. Gale, G. W.; Cui, H.; Reinhardt, K. A., Aqueous cleaning and surface conditioning processes. In *Handbook of Silicon Wafer Cleaning Technology (Third Edition)*, Elsevier: 2018; pp 185-252.
31. Zhou, G.; Niepel, M.; Saretia, S.; Groth, T., Reducing the inflammatory responses of biomaterials by surface modification with glycosaminoglycan multilayers. *Journal of biomedical materials research. Part A* **2016,** *104* (2), 493.
32. Schasfoort, R. B., *Handbook of surface plasmon resonance*. Royal Society of Chemistry: 2017.
33. Halthur, T. J.; Elofsson, U. M., Multilayers of charged polypeptides as studied by in situ ellipsometry and quartz crystal microbalance with dissipation. *Langmuir* **2004,** *20* (5), 1739-1745.
34. Sader, J. E.; Chon, J. W.; Mulvaney, P., Calibration of rectangular atomic force microscope cantilevers. *Review of Scientific Instruments* **1999,** *70* (10), 3967-3969.
35. Renger, A., Johnson, KL, Contact Mechanics. Cambridge etc., Cambridge University Press 1985. XII, 452 pp.,£ 17.50 P/B. ISBN 0521347963. *ZAMM-Journal of Applied Mathematics and Mechanics/Zeitschrift für Angewandte Mathematik und Mechanik* **1989,** *69* (7), 214-214.
36. Zhou, G.; Niepel, M. S.; Saretia, S.; Groth, T., Reducing the inflammatory responses of biomaterials by surface modification with glycosaminoglycan multilayers. *Journal of Biomedical Materials Research Part A* **2016,** *104* (2), 493-502.
37. López-Pérez, P. M.; Marques, A. P.; da Silva, R. M.; Pashkuleva, I.; Reis, R. L., Effect of chitosan membrane surface modification via plasma induced polymerization on the adhesion of osteoblast-like cells. *Journal of Materials Chemistry* **2007,** *17* (38), 4064-4071.
38. Ciancaleoni, G., Lewis Base Activation of Lewis Acid: A Detailed Bond Analysis. *ACS omega* **2018,** *3* (11), 16292-16300.
39. Rodrigues Silva, D.; de Azevedo Santos, L.; Freitas, M. P.; Guerra, C. F.; Hamlin, T. A., Nature and Strength of Lewis Acid/Base Interaction in Boron and Nitrogen Trihalides. *Chemistry–An Asian Journal* **2020,** *15* (23), 4043-4054.
40. Smitha, B.; Sridhar, S.; Khan, A., Chitosan–sodium alginate polyion complexes as fuel cell membranes. *European Polymer Journal* **2005,** *41* (8), 1859-1866.
41. Lawrie, G.; Keen, I.; Drew, B.; Chandler-Temple, A.; Rintoul, L.; Fredericks, P.; Grøndahl, L., Interactions between alginate and chitosan biopolymers characterized using FTIR and XPS. *Biomacromolecules* **2007,** *8* (8), 2533-2541.
42. Cardenas, G.; Miranda, S. P., FTIR and TGA studies of chitosan composite films. *Journal of the Chilean Chemical Society* **2004,** *49* (4), 291-295.
43. Qu, J.; Hu, Q.; Shen, K.; Zhang, K.; Li, Y.; Li, H.; Zhang, Q.; Wang, J.; Quan, W., The preparation and characterization of chitosan rods modified with Fe3+ by a chelation mechanism. *Carbohydrate research* **2011,** *346* (6), 822-827.
44. Lewandowska, K., Miscibility Studies of Hyaluronic Acid and Poly (Vinyl Alcohol) Blends in Various Solvents. *Materials* **2020,** *13* (21), 4750.
45. Lee, E. J.; Kang, E.; Kang, S.-W.; Huh, K. M., Thermo-Irreversible Glycol Chitosan/Hyaluronic Acid Blend Hydrogel for Injectable Tissue Engineering. *Carbohydrate Polymers* **2020**, 116432.
46. Haxaire, K.; Marechal, Y.; Milas, M.; Rinaudo, M., Hydration of polysaccharide hyaluronan observed by IR spectrometry. I. Preliminary experiments and band assignments. *Biopolymers: Original Research on Biomolecules* **2003,** *72* (1), 10-20.
47. Ogawa, K.; Oka, K.; Yui, T., X-ray study of chitosan-transition metal complexes. *Chemistry of materials* **1993,** *5* (5), 726-728.
48. Gritsch, L.; Lovell, C.; Goldmann, W. H.; Boccaccini, A. R., Fabrication and characterization of copper (II)-chitosan complexes as antibiotic-free antibacterial biomaterial. *Carbohydrate polymers* **2018,** *179*, 370-378.

49. Chi, H.; Cao, L.; Wang, J., Synthesis of cross-linked copolymers of the (3-(2-pyridyl) acrylic acid)–copper (ii) complex in supercritical carbon dioxide for the catalytic oxidation of benzyl alcohol. *RSC advances* **2016,** *6* (6), 4434-4441.
50. Song, W.; Mano, J. F., Interactions between cells or proteins and surfaces exhibiting extreme wettabilities. *Soft Matter* **2013,** *9* (11), 2985-2999.
51. Yamanlar, S.; Sant, S.; Boudou, T.; Picart, C.; Khademhosseini, A., Surface functionalization of hyaluronic acid hydrogels by polyelectrolyte multilayer films. *Biomaterials* **2011,** *32* (24), 5590-5599.
52. Apte, G.; Repanas, A.; Willems, C.; Mujtaba, A.; Schmelzer, C. E.; Raichur, A.; Syrowatka, F.; Groth, T., Effect of Different Crosslinking Strategies on Physical Properties and Biocompatibility of Freestanding Multilayer Films Made of Alginate and Chitosan. *Macromolecular Bioscience* **2019,** *19* (11), 1900181.
53. Duval, J. F.; Küttner, D.; Werner, C.; Zimmermann, R., Electrohydrodynamics of soft polyelectrolyte multilayers: point of zero-streaming current. *Langmuir* **2011,** *27* (17), 10739-10752.
54. Aggarwal, N.; Altgärde, N.; Svedhem, S.; Michanetzis, G.; Missirlis, Y.; Groth, T., Tuning Cell Adhesion and Growth on Biomimetic Polyelectrolyte Multilayers by Variation of p H During Layer-by-L ayer Assembly. *Macromolecular bioscience* **2013,** *13* (10), 1327-1338.
55. McNaught, A. D.; Wilkinson, A., *Compendium of chemical terminology*. Blackwell Science Oxford: 1997; Vol. 1669.
56. Nolte, A. J.; Rubner, M. F.; Cohen, R. E., Determining the Young's modulus of polyelectrolyte multilayer films via stress-induced mechanical buckling instabilities. *Macromolecules* **2005,** *38* (13), 5367-5370.
57. Huang, X.; Schubert, A. B.; Chrisman, J. D.; Zacharia, N. S., Formation and tunable disassembly of polyelectrolyte–Cu2+ layer-by-layer complex film. *Langmuir* **2013,** *29* (42), 12959-12968.
58. Kalbitzer, L.; Franke, K.; Möller, S.; Schnabelrauch, M.; Pompe, T., Glycosaminoglycan functionalization of mechanically and topologically defined collagen I matrices. *Journal of Materials Chemistry B* **2015,** *3* (45), 8902-8910.
59. Wagener, V.; Faltz, A.-S.; Killian, M. S.; Schmuki, P.; Virtanen, S., Protein interactions with corroding metal surfaces: comparison of Mg and Fe. *Faraday discussions* **2015,** *180*, 347-360.
60. Balabushevich, N.; De Guerenu, A. L.; Feoktistova, N.; Volodkin, D., Protein loading into porous CaCO 3 microspheres: adsorption equilibrium and bioactivity retention. *Physical Chemistry Chemical Physics* **2015,** *17* (4), 2523-2530.
61. Shi, S.-F.; Jia, J.-F.; Guo, X.-K.; Zhao, Y.-P.; Chen, D.-S.; Guo, Y.-Y.; Cheng, T.; Zhang, X.-L., Biocompatibility of chitosan-coated iron oxide nanoparticles with osteoblast cells. *International journal of nanomedicine* **2012,** *7*, 5593.
62. Kim, B.-E.; Nevitt, T.; Thiele, D. J., Mechanisms for copper acquisition, distribution and regulation. *Nature chemical biology* **2008,** *4* (3), 176-185.
63. Rankin, K. S.; Frankel, D., Hyaluronan in cancer–from the naked mole rat to nanoparticle therapy. *Soft matter* **2016,** *12* (17), 3841-3848.
64. Bird, A. J., Cellular sensing and transport of metal ions: implications in micronutrient homeostasis. *The Journal of nutritional biochemistry* **2015,** *26* (11), 1103-1115.
65. Yoo, H. I.; Moon, Y. H.; Kim, M. S., Effects of CoCl2 on multi-lineage differentiation of C3H/10T1/2 mesenchymal stem cells. *The Korean journal of physiology & pharmacology: official journal of the Korean Physiological Society and the Korean Society of Pharmacology* **2016,** *20* (1), 53.
66. Zhu, Y.; Kruglikov, I. L.; Akgul, Y.; Scherer, P. E., Hyaluronan in adipogenesis, adipose tissue physiology and systemic metabolism. *Matrix Biology* **2019,** *78*, 284-291.
67. Yang, H. The Relationship Between Copper Homeostasis and Lipid Metabolism. Johns Hopkins University, 2018.
68. Festa, M.; Ricciardelli, G.; Mele, G.; Pietropaolo, C.; Ruffo, A.; Colonna, A., Overexpression of H ferritin and up-regulation of iron regulatory protein genes during differentiation of 3T3-L1 pre-adipocytes. *Journal of Biological Chemistry* **2000,** *275* (47), 36708-36712.

69. Bae, Y. K.; Kwon, J. H.; Kim, M.; Kim, G.-H.; Choi, S. J.; Oh, W.; Yang, Y. S.; Jin, H. J.; Jeon, H. B., Intracellular calcium determines the adipogenic differentiation potential of human umbilical cord blood-derived Mesenchymal stem cells via the Wnt5a/β-Catenin signaling pathway. *Stem cells international* **2018,** *2018*.
70. McBeath, R.; Pirone, D. M.; Nelson, C. M.; Bhadriraju, K.; Chen, C. S., Cell shape, cytoskeletal tension, and RhoA regulate stem cell lineage commitment. *Developmental cell* **2004,** *6* (4), 483-495.